

1995

Chemical denaturation of bovine pancreatic Ribonuclease A : monohydric alcohol-mediated denaturation

Sujatha Subbiah
San Jose State University

Follow this and additional works at: https://scholarworks.sjsu.edu/etd_theses

Recommended Citation

Subbiah, Sujatha, "Chemical denaturation of bovine pancreatic Ribonuclease A : monohydric alcohol-mediated denaturation" (1995). *Master's Theses*. 1101.

DOI: <https://doi.org/10.31979/etd.z75r-tzk9>

https://scholarworks.sjsu.edu/etd_theses/1101

This Thesis is brought to you for free and open access by the Master's Theses and Graduate Research at SJSU ScholarWorks. It has been accepted for inclusion in Master's Theses by an authorized administrator of SJSU ScholarWorks. For more information, please contact scholarworks@sjsu.edu.

INFORMATION TO USERS

This manuscript has been reproduced from the microfilm master. UMI films the text directly from the original or copy submitted. Thus, some thesis and dissertation copies are in typewriter face, while others may be from any type of computer printer.

The quality of this reproduction is dependent upon the quality of the copy submitted. Broken or indistinct print, colored or poor quality illustrations and photographs, print bleedthrough, substandard margins, and improper alignment can adversely affect reproduction.

In the unlikely event that the author did not send UMI a complete manuscript and there are missing pages, these will be noted. Also, if unauthorized copyright material had to be removed, a note will indicate the deletion.

Oversize materials (e.g., maps, drawings, charts) are reproduced by sectioning the original, beginning at the upper left-hand corner and continuing from left to right in equal sections with small overlaps. Each original is also photographed in one exposure and is included in reduced form at the back of the book.

Photographs included in the original manuscript have been reproduced xerographically in this copy. Higher quality 6" x 9" black and white photographic prints are available for any photographs or illustrations appearing in this copy for an additional charge. Contact UMI directly to order.

UMI

A Bell & Howell Information Company
300 North Zeeb Road, Ann Arbor, MI 48106-1346 USA
313/761-4700 800/521-0600

**CHEMICAL DENATURATION OF BOVINE PANCREATIC
RIBONUCLEASE A: MONOHYDRIC ALCOHOL-MEDIATED
DENATURATION**

**A Thesis
Presented to
The Faculty of the Department of Chemistry
San Jose State University**

**In Partial Fulfillment
of the Requirements of the Degree
Master of Science**

**by
Sujatha Subbiah
August, 1995**

UMI Number: 1375725

**UMI Microform 1375725
Copyright 1995, by UMI Company. All rights reserved.**

**This microform edition is protected against unauthorized
copying under Title 17, United States Code.**

UMI

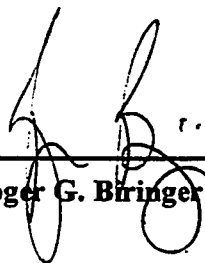
**300 North Zeeb Road
Ann Arbor, MI 48103**

©1995

Sujatha Subbiah

ALL RIGHTS RESERVED

APPROVED FOR THE DEPARTMENT OF CHEMISTRY



Dr. Roger G. Bringer



Dr. Pamela C. Stacks



Dr. Roy Okuda



APPROVED FOR THE UNIVERSITY

ABSTRACT

CHEMICAL DENATURATION OF BOVINE PANCREATIC RIBONUCLEASE A: MONOHYDRIC ALCOHOL-MEDIATED DENATURATION

by

Sujatha Subbiah

The importance of the various factors that contribute to the stability of proteins has been the subject of controversy for many years. It is apparent from the vast amount of experimental work that both hydrogen bonding and the hydrophobic effect are the major contributors, but the relative importance of each has yet to be determined. We have examined the concentration-mediated denaturation of bovine pancreatic Ribonuclease A (RNase A) with a series of monohydric alcohols at constant protonic activities, $p_{a_{H^+}}$ of 3.00 and 4.00. Transition midpoints decrease with increasing hydrophobicity of the alcohol. Denaturation under all conditions yield the expected increase in fluorescence emission. Analysis of these transitions reveals that they do not fit the two-state model. Denaturation with propanols at $p_{a_{H^+}}$ 4.00 give the expected change in the CD signals whereas the corresponding methanol data shows little change. Denaturation with all alcohols at $p_{a_{H^+}}$ 3.00 show an increase in the amplitude of the CD signal. This indicates that an increase in secondary structure accompanies the loss of tertiary structure under these conditions.

ACKNOWLEDGMENTS

I would like to thank Dr. Biringer for his valuable and scholarly guidance. In addition, it is my pleasure to express my thanks to Dr. Pam Stacks and Dr. Roy Okuda for their suggestions on my thesis.

It is with a deep sense of gratitude that I thank my parents for their motivation throughout my school career, and my husband Raja, for his kind assistance, encouragement, and moral support throughout the course of this study.

TABLE OF CONTENTS

	Page
Abstract.....	iv
Acknowledgment.....	v
List of Tables.....	ix
List of Figures.....	x
List of Abbreviations.....	xii
1. INTRODUCTION.....	1
1.1. Protein Structure.....	1
1.2. Significance of Protein Folding.....	2
1.3. Conformational States of Proteins.....	3
1.4. Dominant Forces in Protein Folding.....	5
1.5. Models of Protein Folding.....	13
1.6. Examining Protein Folding by Empirical Methods.....	20
1.7. Background and Significance.....	28
1.8 RNase A as a Model for Protein Folding.....	31
2. MATERIALS AND METHODS.....	33
2.1 Materials.....	33
2.2. Purification of RNase A.....	33

2.3. Determination of $p_{a_{H^+}}$ for Aqueous/Alcohol Solutions.....	33
2.4. Aqueous Standard Curve.....	34
2.5. Determination of $p_{a_{H^+}}$ for Aqueous/Alcohol Solutions.....	36
2.6. Examination of Protocols for Preparation of Alcohol Dilution Series.....	36
2.7. Preparation of Protein Stock Solutions.....	37
2.8. Preparation of Alcohol Dilution Series.....	38
2.9. Fluorescence-Monitored Chemically-Induced Denaturation Transitions.....	39
2.10. CD-monitored Chemically-Induced Denaturation Transitions.....	40
2.11. Data Analysis.....	43
2.12. Evaluation of the Thermodynamic Parameters.....	48
3. RESULTS.....	49
3.1. Protonic Activity for Aqueous/Alcohol Solutions.....	49
3.2. Denaturation of RNase A by Monohydric Alcohols.....	52
3.3. Aggregation.....	65
3.4. Singular Value Decomposition Analysis.....	65
4. DISCUSSION.....	68
4.1. Fluorescence Studies.....	68
4.2. Transition Midpoints.....	68
4.3. Circular Dichroism Studies.....	71

4.4. Singular Value Decomposition Analysis.....	73
4.5. Aggregation.....	74
5. CONCLUSIONS.....	76
REFERENCES.....	77

LIST OF TABLES

Table	Page
1. Transition Midpoints.....	69

LIST OF FIGURES

Figures	Page
1. Diffusion-collision model.....	16
2. Molten globule model.....	18
3. Hydrophobic zipper model.....	19
4. Typical denaturation curve.....	26
5. Alkylurea studies.....	30
6. Data analysis.....	45
7. Free energy vs F_u curve.....	46
8. Aqueous standard curve at pH 3.00.....	50
9. Aqueous standard curve at pH 4.00.....	51
10. Final pH vs M for methanol.....	53
11. Final pH vs M for 1-propanol.....	54
12. Final pH vs M for 2-propanol.....	55
13. Fluorescence and CD of methanol at $p_{a_{H^+}}$ 3.00.....	56
14. Fluorescence and CD of methanol at $p_{a_{H^+}}$ 4.00.....	57
15. Fluorescence-monitored denaturation of methanol.....	59
16. Fluorescence and CD of 1-propanol at $p_{a_{H^+}}$ 3.00.....	61
17. Fluorescence and CD of 1-propanol at $p_{a_{H^+}}$ 4.00.....	62
18. Fluorescence and CD of 2-propanol at $p_{a_{H^+}}$ 3.00.....	63

19. Fluorescence and CD of 2-propanol at p_{H^+} 4.00.....	64
20. Singular value decomposition data.....	66

LIST OF ABBREVIATIONS

ΔG	Change in free energy
2,6-DNP	Dinitrophenol
BPTI	Bovine pancreatic trypsin inhibitor
A	Compact intermediate state
CD	Circular dichroism
C_m	Concentration midpoint
CSA	Camphor sulfonic acid
Far UV-CD	Far ultraviolet circular dichroism
GdmCl	Guanidinium chloride
N	Native state of RNase A
NMR	Nuclear magnetic resonance
p_{aH^+}	- log Protonic activity
RNase A	Bovine pancreatic Ribonuclease A
RNase T1	Ribonuclease T1
SF	Scaling factor
SVD	Singular value decomposition analysis
U	Unfolded state of RNase A
UV	Ultraviolet

1. INTRODUCTION

1.1 Protein Structure

In all areas of biological and medical research today, there is an increasing need for a thorough knowledge of protein structure and function. Proteins are complex biological macromolecules, and, in essence, are the “building blocks” of life. Proteins play a crucial role in many biological processes such as, enzyme catalysis, transport and storage, mechanical support, immune protection and coordinated motion.

Proteins are built from a “repertoire” of twenty different amino acids. These amino acids, upon polymerization, eliminate a molecule of water to form the CO-NH linkage known as the “peptide bond.” Proteins consist of one or more of these polypeptide chains. The functions of proteins can be understood in terms of their structure, the three-dimensional relationship between the component atoms (Creighton, 1990).

Proteins have four levels of structural organization. The primary structure of proteins represents the amino acid sequence of the polypeptide chains. The secondary structure represents the localized spatial arrangement of a polypeptide backbone that is stabilized by hydrogen bonds. Helices, pleated sheets and turns are some of the regular polypeptide folding patterns. Tertiary structure refers to the packaging of the secondary structure. Some proteins are composed of two or more independent polypeptide chains known as subunits. The quaternary structure of protein refers to the spatial arrangement of these subunits (Creighton, 1990).

1.2 Significance of Protein Folding

An understanding of how proteins fold is of major biological significance. Protein folding is the process by which a polypeptide chain attains the highly structured state of the native protein. To be biologically active, all the proteins must adopt specific folded three-dimensional structures. The fact that proteins with a given amino acid sequence always attain the same native structure and different sequences lead to different structures indicates that the amino acid sequence “codes” for the native protein structure. Deciphering this “code” is known as the protein folding problem. Knowledge of this folding “code” will allow for the direct translation of the amino acid sequences into three-dimensional structures.

Knowledge of the protein folding “code” is paramount to the interpretation of results obtained from the Human Genome Project. The essence of the relationship between the protein folding “code” and the Human Genome Project is perhaps best captured by the title to an address given by Charles Cantor, “Once we have the human genome map we will know how to fold it.” The Human Genome Project will yield a plethora of amino acid sequences for proteins with unknown structure and function.

The mechanism of protein folding has been studied by many researchers in order to gain information about the relationship between the primary and native three-dimensional structure of proteins (Creighton, T. E., 1990; Matthews, C. R., 1993). Several models have been proposed to define the process of protein folding. Some assume that folding is the result of random fluctuations of the polypeptide chain. Others suggest that the pathway of protein folding is dominated by the existence of native like, “molten globule”

states as intermediates. Still, others postulate that protein folding is a sequential process governed by a series of well defined intermediates. Current interest in the mechanisms and pathways of protein folding are centered around the proteins that exhibit multi state folding transitions. All the models chosen to describe the folding process involve the definitive characterization of the native, unfolded and partially folded structures. From a comparison of a number of such structures, the folding pathway can be deduced. The characterization of the intermediate states along the multi state transitions serve as excellent tools for understanding the mechanism and pathway of folding (Biringer and Fink, 1982).

1.3 Conformational States of Proteins

1.3.1 Native, Fully Folded State (N):

The native conformations of many proteins are known in great detail from the structures determined by x-ray crystallography and NMR studies. To be biologically active, proteins must adopt specific three-dimensional structures upon folding. As noted above, the primary sequence defines the final folded state. Hence, the polypeptide backbone does not require extrinsic factors or input of energy to attain this fully folded conformation. The folding of this polypeptide chain into a specific three-dimensional structure is a reversible process for most globular proteins. The folded state of the proteins are only marginally stable and may be disrupted by changes in temperature, pH, or by the addition of a variety of different denaturants. The native state is the result of a subtle balance between a number of noncovalent interactions. The native structure is compact and highly ordered as compared to the unfolded “random” polypeptide chain

from which it was formed.

1.3.2 Unfolded State (U):

The unfolded state of a protein is considered to be a random polypeptide coil in which the rotation about every chemical bond of the polypeptide is independent of every other bond rotation and determined only by the local stereochemistry of the polypeptide backbone. The unfolded or denatured state of a protein has no definite structure, but has a very labile fluctuating conformation. Dill and Shortle (1991), have performed extensive research on the denatured state of the proteins. They found that proteins unfolded in the presence of strong denaturants such as 6 M Guanidinium chloride (GdmCl) or 8 M urea have the hydrodynamic properties expected for random coil polypeptides.

1.3.3 "Molten Globule," a Compact Intermediate State:

Under particular conditions of pH, salt, and temperature, a variety of proteins have been shown to exist in stable conformations that are neither fully folded nor fully unfolded. The term "molten globule" was introduced to explain the occurrence of conformations with native like secondary structure and a liquidlike interior. This compact intermediate state lacks native tertiary structure. The molten globule state was first predicted as a potential kinetic intermediate in protein folding pathway for small globular proteins (Kuwajima, 1989). In this state, the interior side chains are in homogenous surroundings, in contrast to the asymmetric environments they have in the fully folded state.

Many studies have been carried out to characterize the role of the molten globule state in the folding of proteins (Ptitsyn, 1992). Fink et al. (1994) have investigated the

acid-induced unfolding of 20 small monomeric proteins as a function of ionic strength. Some proteins, upon the addition of acid at low pH's, initially unfold and then refold into a compact or expanded molten globulelike conformation known as the acid-denatured or A state. The A state exhibits a high level of secondary structure and minimal tertiary structure. The conformational properties of the A state have been extensively studied by Ptitsyn (1992) and Goto et al. (1990). The A state adheres to the definition of a molten globule on the basis of compactness and amount of the secondary structure (Ptitsyn, 1992).

1.4 Dominant Forces Involved In Protein Folding

1.4.1 General Aspects

The folded states of proteins are only marginally more stable than the fully unfolded state under physiological conditions. The free energy difference (ΔG_{unfold}) between these states is only 5-20 kcal/mol, which is less than 1/10 kT per residue, where k is the Boltzmann's constant and T is the temperature (Dill, 1990).

$$\Delta G_{\text{unfold}} = G_{\text{denatured}} - G_{\text{native}} \quad (1)$$

Many types of molecular interactions contribute to the stability. Consequently, a protein's structure is the result of a delicate balance between many different enthalpic and entropic countervailing contributions. The noncovalent forces involved include: electrostatic interactions, hydrogen bonding and van der Waals interactions, and hydrophobic interactions.

The complex collection of the forces that determine the native configuration of the

protein must necessarily be reflected in protein folding pathway and thus each interaction has a role to play in the overall process. Owing to the extreme complexities involved in the folding process, it is not currently known whether folding is driven mainly by thermodynamics or by kinetics or by a combination of the two. The relative importance of these interactions is the center of considerable controversy. In the following sections the nature of these forces and their contribution towards protein stability are discussed (Dill, 1990).

1.4.2 Electrostatic Interactions

Prior to the application of x-ray crystallography to protein structure determination, the folding forces were assumed to be purely electrostatic in nature, as acids and bases were among the earliest known protein denaturants. The electrostatic interaction forces depend on the number and distribution of the charges, and, therefore, differ in the native and unfolded states of the protein. Addition of acids or bases cause changes in the pH that can result in a change in the ionization state of acidic or basic side chains. The particular charge associated with a particular side chain depends on the pH relative to its pK. Further, the pK of a side chain can be altered by its environment. In fact, buried groups can have a pK change of one or more units depending on the environment. Since the solvent exposure in the native state differs from that in the unfolded state, the pK values of the ionizable groups may be different for the different states. The ionization state of side chains can affect the conformational stability of a globular protein in two ways: (1) “Specific” electrostatic attractions and (2) “Classical” electrostatic repulsion. The overall stability is defined by the difference between the sum of the attractive and the repulsive

interactions in the folded and unfolded conformations of the protein.

“Classical” electrostatic effects are the nonspecific repulsions that arise when a protein is highly charged. Proteins at their isoelectric points (pI) have equal amounts of positive and negative charges. At pH values above or below the pI, the protein will have an excess of negative or positive charges respectively. The greater the difference between the pH and pI, the larger the overall charge will be. At very high overall charge, the repulsive forces may lead to denaturation of the protein, as the charge separation will be larger in the unfolded state. Pace et al. (1990) have investigated the pH dependence of the urea and guanidinium chloride (GdmCl) denaturation of RNase A and RNase T1 (*Aspergillus oryzae*). Their results show these proteins are most stable near their pI and the electrostatic interactions among charged groups make a small contribution towards the conformational stabilities of these proteins.

The second interaction that affects protein stability is the “specific” charge interactions. An ion pair or salt bridge is formed by the attraction between two oppositely charged side chains. During the 1930's, ion pairs were considered to be the dominant contributor to protein stability. This has since been called into question. The protein stability due to these ion pairs arises from the charged pairs buried on the core of the protein. X-ray crystal studies of known proteins suggest that ion pairing on the surface of the protein contributes to protein stability (Jaenicke, 1991). However, it is difficult to discriminate between classical and ion pairing electrostatics towards protein stability (Jaenicke, 1991, Seckler and Jaenicke, 1991).

Several researchers suggest that ionic interactions are strong but do not greatly

stabilize proteins (Tanford, 1968; Stigter and Dill, 1990; Pace et al. 1990). They conclude that ion pairing is not the dominant force in the folding of most small globular proteins, as only a very few ion pairs are buried within the core of most globular proteins and since ion pairs exposed to aqueous solvent are poorly conserved. However, recent studies by Dym et al. (1995) suggest that ion pairs are abundant and stronger in the proteins of thermophilic organisms and are major contributors to these proteins' thermostability.

Stigter and Dill (1990), explained the role of ion pairs using a polyelectrolyte model for proteins. They conclude that increasing salt will reduce the electrostatic free energy of the unfolded state of myoglobin more than the folded state, as increased salt will shield the charge repulsions in the unfolded molecule more effectively than in the folded molecule. They suggest that this is due to a better penetration of the salt solution into the unfolded molecule. Experiments on the pH dependence of the free energy of stabilization of RNase A and RNase T1 (*Aspergillus oryzae*) against urea denaturation were carried out by Pace et al. (1990). Their results indicate that electrostatic interactions among the charged groups make a contribution towards conformational stability of both proteins.

1.4.3 Hydrogen Bonding and van der Waals Interactions

Hydrogen bonds and van der Waals interactions are involved in the stabilization of native protein structure and influence the protein folding pathway. Hydrogen bonds also play a significant role in conferring the structural specificity to the native state of the protein. The intrinsic energy of a hydrogen bond is usually -2 to -8 kcal/mol and the strength decreases as the distance between the hydrogen bond donor and acceptor

increases. The van der Waals attractions arise from the electrostatic interactions among fixed or induced dipoles.

Most hydrogen bonding in proteins occurs between the carbonyl C=O and amide hydrogens of the peptide backbone. The hydrogen bond between the peptide carbonyl and amide groups of the backbone is important in proteins, as it stabilizes regular structures such as α -helices, β -structures, and turns. However, some amino acid side-chains are dipolar and hence are capable of hydrogen bonding. In addition, the polar side chains located on the outside of the molecule can form hydrogen bonds with neighboring water molecules. The internal hydrogen bonding groups within a protein are arranged in a fashion such that nearly all possible hydrogen bonds are formed and provide a structural basis for the native pattern of folding.

Denaturation studies conducted by Singer (1962) with non-aqueous solvents suggest that hydrogen bonding is not the dominant force in protein folding. In general, the peptide carbonyl group is a strong hydrogen acceptor and the peptide amino group is a weak hydrogen donor. Singer pointed out that solvents useful for competing with the peptide hydrogen bond must be stronger hydrogen donors than the amide group and stronger hydrogen acceptors than the carbonyl group. For example, dioxane being a weak hydrogen bond acceptor should not denature proteins, if hydrogen bonding is the dominant force. However, dioxane has been shown to denature proteins (Singer, 1962).

The current popular view is that both hydrogen bonding and van der Waals interactions play a minor role in the stabilization of the native protein structure, although they might be more important in directing protein folding. According to Creighton,

“within the polar aqueous environment, noncovalent interactions between different parts of the polypeptide chain, by electrostatic interactions, hydrogen bonds or van der Waals forces are not expected to be especially favorable energetically, because similar interactions will occur between the polypeptide and the water surrounding it” (Creighton and Goldenberg, 1984).

1.4.4 Hydrophobic Interactions

It is presently thought that the stabilization of the native compact protein structure is primarily due to hydrophobic interactions. In addition, it is generally accepted that hydrophobic interactions are important in directing protein folding. The term ‘hydrophobic interactions’ means different things to different people and it is too often misunderstood. It is most useful to define the hydrophobic effect in terms of the free energy of solvation. To facilitate solvation of apolar compounds, water molecules form a highly ordered cavity in which the apolar solute will fit. Although solvation is enthalpically favored, the entropy that is associated with the “ordering” of water molecules is unfavorable at ambient temperatures. Since, the overall free energy is dominated by entropy ($T\Delta S \gg \Delta H$), the associated Gibbs free energy (ΔG) for the process becomes positive, opposing solvation (Privalov and Gill, 1989).

The unfavorable entropy associated with the solvent exposure of hydrophobic groups explains why most nonpolar residues are located in the interior where they are shielded from the solvent, while the most polar and charged amino acid residues are present at the surface of native proteins. This coalescence of the nonpolar residues to form

the “hydrophobic core” serves to minimize the solvent entropy and, in this way, stabilize the native conformation.

The hydrophobic effect not only stabilizes the protein structure, but also drives proteins to form compact structures. The hydrophobic groups that are exposed on the denatured polypeptides serve to order water molecules and hence decrease solvent entropy. Compaction serves to bury such hydrophobic groups resulting in an increase in solvent entropy and hence, an overall reduction in the free energy of the solution. The solvent-driven compaction is opposed by the unfavorable change in solute entropy which arises due to the localization of nonpolar residues in the compact, hydrophobic protein core. The difference between these two large, opposing forces is small with a ΔG of -10 kcal/mol for small proteins (Creighton, 1990).

Dill (1990) has examined the compaction of the polypeptides through computer modeling using a “lattice model.” He observed that compaction of polypeptides into regular folded patterns yielded a higher solute entropy than if the polypeptides were folded randomly. This means that the solute entropy decrease is less for ordered compaction and will thus be the preferred mode for compaction.

1.4.5 Evidence for the Hydrophobic Interactions

A number of studies give experimental evidence that support the hypothesis that hydrophobic interactions are important driving forces in protein folding. Singer (1962) has shown that nonpolar solvents can denature proteins. To explain these results, Singer proposed that the nonpolar solvent reduces the free energy of the unfolded state by

solvating the exposed nonpolar amino acids.

A second piece of supporting evidence was reported by von Hippel and Schleich (1969). They observed that the ability of a particular ion to destabilize protein structure was directly related to its ability to enhance the water solubility of hydrophobic compounds. Since the denatured state has more solvent exposed hydrophobic groups than the native state, ions that enhance the solubility of hydrophobic side chains would necessarily lower the free energy of the denatured state and, in this way, promote denaturation.

Brandts and Hunt (1967), have shown that there are prominent effects on the thermodynamics of denaturation brought by the presence of ethanol. Comparison of the experimental folding thermodynamics for RNase A in water to that in aqueous/ethanol suggests that conformational stability is associated with the solvation of hydrophobic side chains in the denatured state. Since hydrophobic groups are buried in folded structures and solvent exposed in denatured structures, conditions that favor the solvation of the hydrophobic groups necessarily favor the formation of the denatured state over the native state.

1.4.5 Concluding Remarks

A delicate balance between hydrophobic, hydrogen bonding and electrostatic interactions contribute to the stability of proteins. The complex collection of forces that determine the native configuration of the protein must surely be reflected in protein folding and hence each interaction plays a role in guiding the overall folding process. The relative importance of hydrogen bonding and the hydrophobic effect in the stabilization of

proteins is the subject of considerable controversy. Based on several studies, one arrives at the conclusion that stabilization of the native compact protein structure is primarily due to the hydrophobic interactions between the nonpolar groups of the protein molecule (Dill, 1990; Ptitsyn, 1992; Creighton, 1990).

1.5 Models for Protein Folding

1.5.1 Introduction

The forces controlling the denaturation and folding of proteins and the mechanisms by which these processes occur have been subject to investigation and controversy for nearly sixty years. Historically, Wu is credited with the modern view that native proteins involve regular repeated patterns of folded polypeptide chain that is organized into a three-dimensional network and held together by noncovalent forces (Dill, 1990). According to Wu, “denaturation is the breaking up of these labile linkages. Instead of being compact, the protein now becomes a diffuse structure. The surface gets altered and the interior of the molecule is exposed” (Wu, 1929).

Experiments reported by Anson (1945) show that hemoglobin folding is reversible as evidenced by similarities in solubility, characteristic absorbance spectra, binding to O₂ and CO, and inaccessibility to trypsin digestion. Later studies have shown that the denaturation of many small globular proteins is reversible and cooperative under certain experimental conditions. The cooperative nature necessarily implies that the folding of small globular proteins can be approximated by a two-state equilibrium model, involving only the native state (N), and the unfolded state (U) (Schmid, 1993).

1.5.2 Random Search Model

Levinthal (1968) examined the possibility that proteins might fold by a purely random search of all possible conformations. He calculated that the time required for folding a protein chain with 100 residues would be nearly 10^{50} years (Schmid, 1993). Thus, even for a very small protein, it would take longer than the age of the known universe to explore all its possible conformations! Levitt (1975) proposed that the number of possible chain conformations is significantly reduced if only self-avoiding conformations are allowed. Creighton (1990) found that random search biased in this manner could occur in the time frame observed for protein folding (0.1-1000 seconds).

1.5.3 Nucleation Rapid Growth Model

The nucleation rapid growth model was proposed by Wetlaufer (1973). According to this model, a nucleation center is formed in the early stages of a folding pathway through random conformational fluctuations of the unfolded protein. The nucleation center serves as a template upon which folding proceeds to rapid completion. Further, the nucleation center is unstable and breaks down if it is not stabilized by further folding and should be small enough to facilitate a random search.

Formation of the nucleation center is the rate-limiting step in this model. Folding intermediates are not populated in this model, as the folding occurs rapidly after the nucleation center is formed. The nucleation rapid growth model does not explain a significant amount of experimental data. In particular, this model does not account for the existence of intermediates observed in the folding of number of proteins.

1.5.4 Diffusion-Collision-Adhesion Model

The diffusion-collision-adhesion model postulates that folding begins with short segments of the unfolded protein chain that fold independently into microdomains of limited stability. Several (two or more) of the microdomains then diffuse together and coalesce into larger structures. The process of folding the entire protein to the native state then involves a series of sequential diffusion-collision steps. A pictorial representation is shown in Figure 1. Karplus and Weaver (1994), calculated the rate for a protein to fold by a diffusion-collision model and found that the diffusional collision to form the microdomains would be the rate-limiting step. However, Kim and Baldwin (1982), have pointed out that coalescence of two microdomains could also be rate-limiting in certain situations.

Kim and Baldwin (1982) studied the kinetics of folding of RNase A as a function of solvent viscosity. They found that the overall folding rate was independent of solvent viscosity and concluded that diffusion is not rate-limiting for the folding of this protein. In contrast, Karplus and Weaver (1994) examined model polymers and found that the diffusion of one segment to another decreased with increasing solvent viscosity, indicating that diffusion is rate limiting for the folding of these polymers.

1.5.5 Molten Globule Model

Kuwajima proposed the molten globule model to describe the structure of intermediates formed early in the folding pathway for small globular proteins. The molten globule model structure is usually characterized by a compact form containing nativelylike

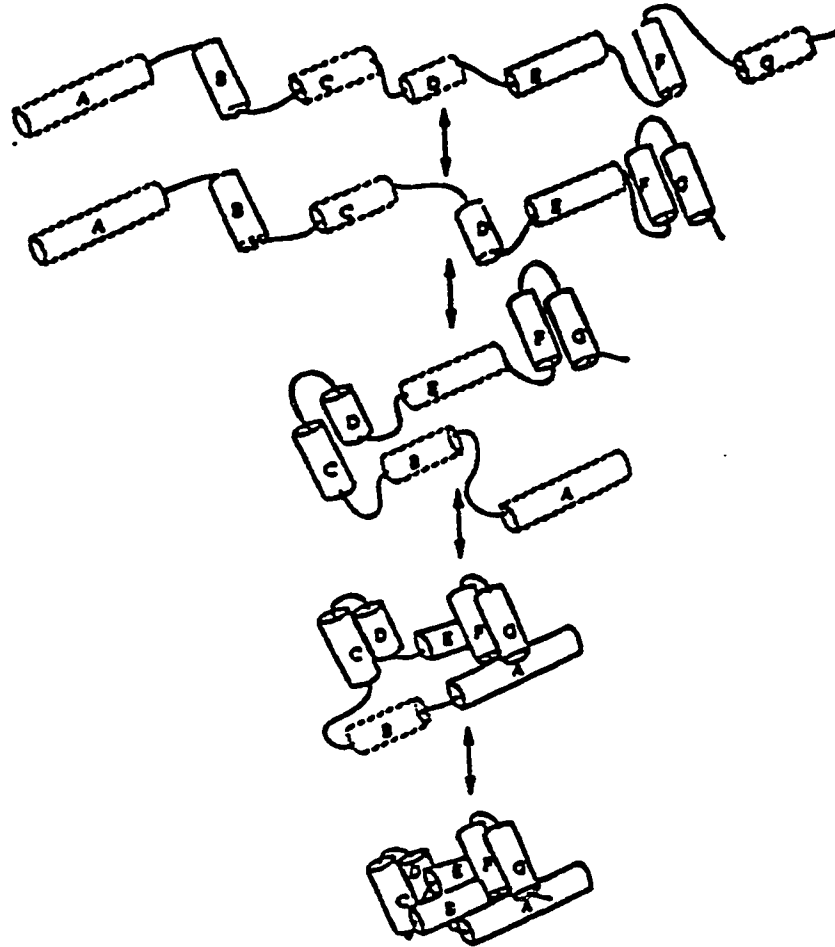


Figure 1: Diffusion-collision model. Pictorial representation of kinetic event involved in the Diffusion-adhesion-collision model of small globular proteins and protein domains. Microdomains (A-G) (indicated by dashed outlines) are individually unstable. Stable coalescent intermediates (indicated by solid outlines) are held together by hydrophobic interactions. Reproduced with permission from Karplus and Weaver, 1994, copyright 1994, by Cambridge University Press.

secondary structures but lacking native tertiary structure. The molten globule state is stabilized by nonspecific hydrophobic interactions between nonpolar residues located in the interior of the structure (Figure 2). It has been proposed that the molten globule state forms early in folding and the rate determining step involves later structural changes after the accumulation of the molten globule state (Kuwajima, 1989).

1.5.6 Hydrophobic Zipper Model

Dill et al. (1993) have proposed that proteins may fold through the hydrophobic zipper model (HZ model). In this model, the hydrophobic contacts act as constraints bringing other such contacts into spatial proximity which constrains the structure further and "zips" up the next contacts (Figure 3). The hydrophobic zipper-heteropolymer collapse is a highly cooperative process driven by nonlocal interactions. Further, the collapse itself results in the formation of sheets, helices and irregular structures.

This model was tested through computer modeling for bovine pancreatic trypsin inhibitor (BPTI) and crammnin. The best structures predicted by this model have energies within about 1.5 kcal/mol of the actual native structures (Dill et al. 1993). Even though the hydrophobic zipper search strategy shows promise, extensive research is necessary to confirm this model.

1.5.7 Sequential Folding Model

According to Kim and Baldwin, folding proceeds in a sequence of unique and finite steps involving the formation of discrete partially-folded structures. Using suitable conditions of folding, the intermediates involved in a protein folding pathway can be populated. There are two variations to this model, the modular assembly model and the

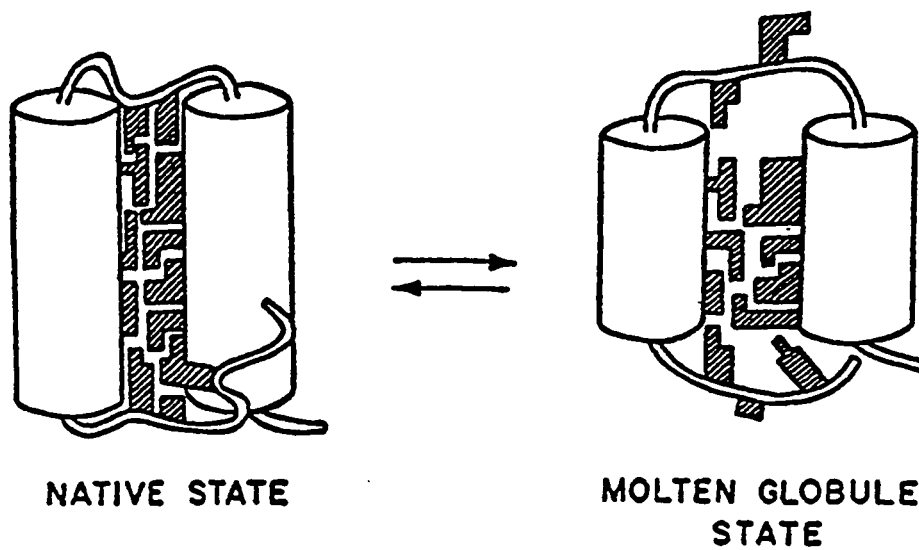


Figure 2: Molten globule model. Schematic representation of the native and molten globule states of the protein molecule. The cylinders represent α -helical structures and nonpolar side chains are represented by the hatched patterns. Reproduced with permission from Ptitsyn, 1992, copyright by W. H. Freeman and Company, 1992.

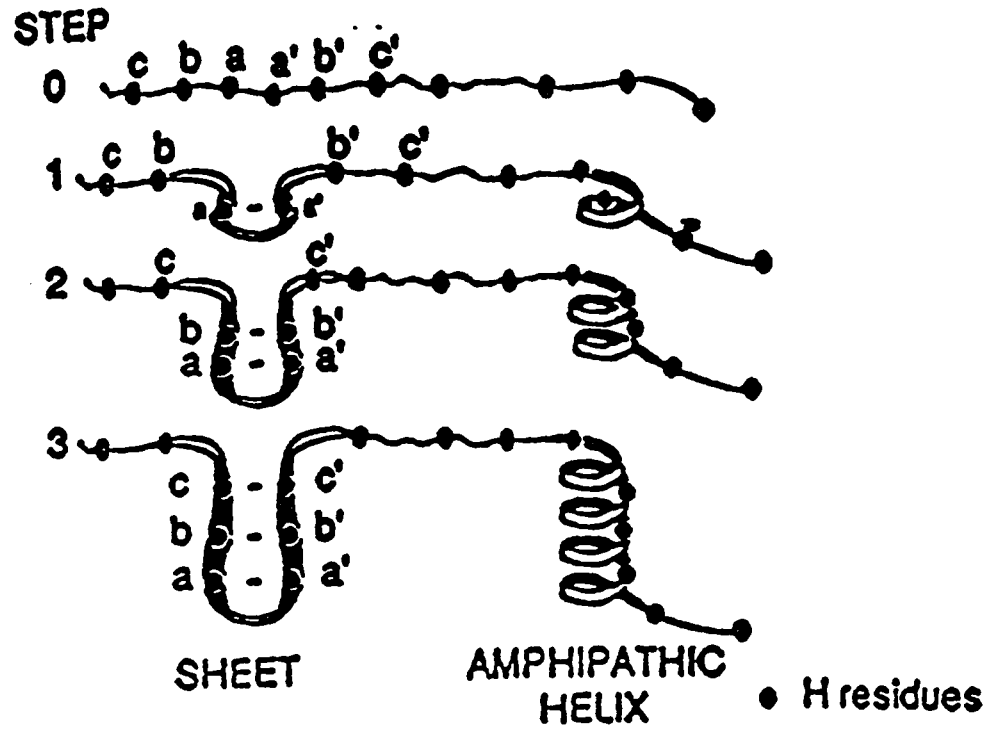


Figure 3: Hydrophobic-zipper model. Schematic representation of the hydrophobic-zipper model. The closest hydrophobic (H) residues (solid dots) in sequence pair first, constrain the chain and bring other H monomers into proximity. As H contacts form, to develop a core, helices and sheets zip up. Reproduced with permission from Dill et al. 1993, copyright National Academy of Sciences USA.

frame work model. The modular assembly model assumes that specific regions of the protein fold independently, but at different times (Baldwin, 1975). In the frame work model, as proposed by Kim and Baldwin (1982), most secondary structure is formed before the formation of the tertiary structure. They proposed that folding begins with the formation of individual transient secondary structural elements that are stabilized by tight packing with other structures. In this model, the folding is a hierarchical process in which simple structures are formed first and these interact to give more complex structures. Experiments performed by Schmid and Baldwin (1979) using the exchange of tritium-labeled amide protons with RNase A lend support to the sequential model.

1.5.8 Concluding Remarks

To conclude, experimental data provides some support for all but the random search model for protein folding, but also provide contradictions. Given the complexity involved in the nature of protein folding, the processes that lead to the native protein from a random polypeptide chain most likely involve elements of many of the proposed models.

1.6 Examining Protein Folding by Empirical Methods

1.6.1 Introduction

Numerous methodologies have been developed to examine the process of protein folding and unfolding. Chief among them are absorbance and fluorescence spectroscopy, which serve to measure the gross three-dimensional structure of the protein, and circular dichroism, which serves to measure the secondary structure. Although these methods have proven invaluable in the study of protein folding, the information that they individually

give do not provide a complete picture of the process. However, a more complete picture of the folding process can be obtained by employing a variety of techniques.

1.6.2 Absorbance and Fluorescence Spectroscopy

Spectral methods are widely used to determine protein stability and to monitor structural transitions, such as in unfolding and refolding of proteins. Absorbance and fluorescence are the two probes used to measure the changes in the environment about the aromatic amino acid residues. A wealth of information about the tertiary structure, and changes in the tertiary structure can be obtained by examining the spectral properties. Absorbance values measured at a given point in the absorption band will be different when the aromatic residues are in the hydrophobic core of the native protein as opposed to when they are exposed to the polar solvent (water) in the unfolded state. The absorbance spectrum for residues buried in the native protein will occur at longer wavelengths than when they are exposed to solvent in the unfolded state as a result of the difference in polarizability between the different environments. In a typical folding or unfolding experiment, the absorbance is monitored on the long wavelength side of the absorbance band. Upon denaturation, the absorbance spectrum will shift to shorter wavelengths and a decrease in absorbance will be observed.

Fluorescence spectroscopy also serves as a valuable tool, as it provides insight into the structure and dynamics of proteins. The aromatic amino acids (tryptophan and tyrosine) act as intrinsic fluorescent probes in proteins. The fluorescence of these side chains is lower when the protein is in the native state than when it is unfolded. This is due to the fact that the tight packing of side chains in the native state provides a more efficient

means for fluorescence-quenching than can occur in the more open structure of the unfolded state. Hence, unfolding is accompanied by an increase in fluorescence and refolding by a decrease in fluorescence. Further, since the excited state lifetime associated with fluorescence is considerably longer than that associated with absorbance, fluorescence spectroscopy is more sensitive to changes in the environment than absorbance spectroscopy. The longer lifetimes allow for the environment to significantly alter the electron distribution about the excited state, and such alterations have a profound effect on the resulting signal. Consequently, fluorescence can detect small changes in structure that are invisible to absorbance measurements (Stryer, 1968).

The fluorescence and absorbance spectra for RNase A provide a measure of the solvent exposure of tyrosine residues; RNase A contains no tryptophan. Upon denaturation, the buried tyrosines within the native structure become solvent exposed, resulting in a change in both the absorbance and fluorescence spectra. The major difference in the absorption spectra occurs at 286 nm where the denatured state absorbance is lower than that of the native state. The major difference in the fluorescence spectra occurs at 305 nm (emission wavelength) with an excitation wavelength of 280 nm, where the fluorescence of the denatured state is higher than the native state.

1.6.3 Circular Dichroism

Circular Dichroism (CD) is a measure of the unequal absorption of left- and right-handed circularly polarized light, a property of chiral molecules. Two spectral regions give different kinds of information about protein structure. The near UV spectra gives

information about the tertiary structure of the proteins. In the near UV region, aromatic side chains absorb strongly. For free amino acids, these rings are not chiral and hence will not produce a CD signal. However, if the side chains are buried in the protein structure, the π -electron cloud can be distorted in a chiral manner. This distortion in the structure produces a CD signal with large amplitude. Upon denaturation of the protein, the distortion will be removed and the CD signal lost.

The far ultraviolet circular dichroism spectra contain a wealth of information about the secondary structure of proteins. In particular, the α -helix displays a high amplitude CD spectrum in the far-UV region. Traditionally, the molar ellipticity at 222 nm has been used as a measure of α -helix content, as it is the major contributor at this wavelength. Compton and Johnson (1986) have shown that α -helix does not contribute to ellipticity at 201 nm and all the other structural elements (e.g., parallel sheet, antiparallel sheet, and turns) will contribute. Thus the ellipticity at 201 nm, provides a measure of secondary structures other than a α -helix.

1.6.4 Proton Nuclear Magnetic Resonance Studies

Nuclear magnetic resonance (NMR) spectroscopy has proven to be a powerful tool for the elucidation of the protein structure as well as for monitoring protein folding. NMR is a particularly useful technique, as it provides a means to monitor the environment about each amino acid residue. The sensitivity of the chemical shifts to the slightest changes in environment make this ideal for characterizing differences between structural states.

Blum et al. (1978), and Biringer and Fink (1982) used the C-2 protons of the four histidine residues (His-12, -48, -105, -119) of RNase A to monitor protein folding. When partially folded intermediates were populated during folding, new transient resonances were observed with chemical shifts that were different from both native and unfolded protein. The thermal unfolding transition in several aqueous/methanol solvent systems has been examined in detail (Biringer and Fink, 1982). The stabilizing effect of the organic cosolvent allowed for the observation and partial characterization of intermediate states.

1.6.5 Equilibrium Measurements

Native proteins can be unfolded by altering the temperature, pH, solvent, or by adding chemical denaturants such that the equilibrium is shifted to favor the unfolded state. Many small single domain proteins unfold reversibly and in a cooperative manner, indicating that partially folded states are not populated. Thus, the folding of small globular proteins can be described by the two-state approximation involving only the native and fully unfolded species. The equilibrium transitions are described by:



where U and N represent the unfolded and native states respectively (Kim and Baldwin 1982; Schmid and Baldwin, 1979). At any point in the transition, the relative population of native and unfolded protein are related by the equilibrium expression:

$$K_{eq} = [U]/[N] \quad (3)$$

Under mild denaturing conditions, the native state remains as the predominant species. But as the stronger denaturing conditions are applied, the denaturation transition is reached

where both the folded and unfolded states coexist, and the equilibrium constant will be closer to unity. With continued change in conditions, there is an increase in the equilibrium constant favoring the unfolded state. The free energy difference (ΔG) between the native and unfolded states, is related to K_{eq} by the following relationship:

$$\Delta G = -RT \ln K_{eq} \quad (4)$$

where R is the universal gas constant and T is the absolute temperature in Kelvin scale.

Figure 4 shows a GdmCl denaturation curve which is typical for two-state folding transitions. The solid line represents the fraction of unfolded molecules, f_u , (right scale from 0 to 1) observed experimentally. Within the transition region (2.8 to 3.2 M GdmCl), the free energy difference (ΔG) between the native and unfolded states varies in a linear fashion with the denaturant concentration. Assuming that change in free energy is linear over all concentrations of the denaturant, the free energy values at concentrations outside the transition region can be obtained¹. Thus, extrapolation of the free energy values to zero denaturant concentration (dashed line in Figure 4) gives the ΔG for the process in the absence of denaturant (ΔG^{so}) (Creighton and Goldenberg, 1984).

For a noncooperative transition, the two-state approximation is not valid, as low levels of partially folded intermediate states which are indistinguishable from either native or unfolded states are observed. In the situation where only one intermediate is populated the equilibrium expression becomes:

¹ This is a typical assumption that works well with urea, but other denaturants may not follow.

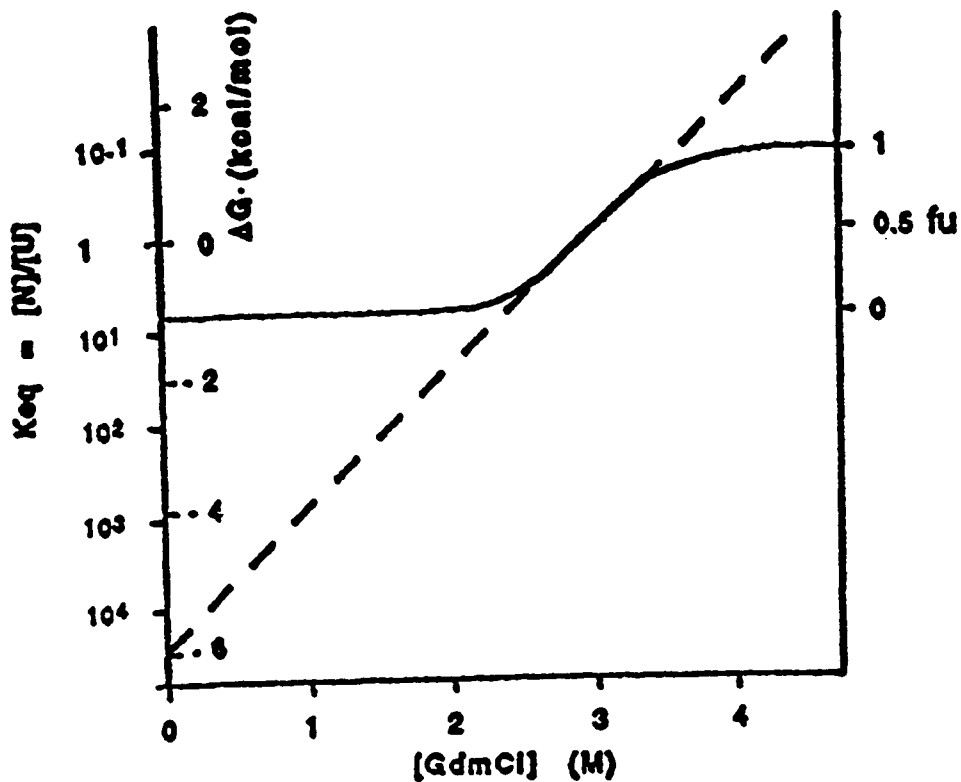


Figure 4: Typical denaturation curve. The solid line gives data as the fraction of unfolded molecules (f_u) versus guanidinium chloride (GdmCl) concentration. The dotted line gives the change in free energy (ΔG) and the log of the equilibrium constant (K_{eq}) versus GdmCl. Reproduced with permission from Creighton and Goldenberg, 1984, copyright Academic Press Limited.



where I represents the population of partially folded intermediates and N and U have the usual meaning. The overall equilibrium constant ($K_{eq \text{ overall}}$) will be a product of the individual equilibria as given by:

$$K_{eq \text{ overall}} = K_1 * K_2 \quad (6)$$

where $K_1 = [I]/[N]$, and $K_2 = [U]/[I]$ respectively. The apparent free energy (ΔG_{app}) is related to K_{eq} as in equation 4 and, in this case, it is a sum of the individual free energies. The plots of ΔG vs M denaturant will necessarily be curved, and are diagnostic for multiple states.

1.6.6 Kinetic Measurements

One approach used to examine the protein folding problem involves the study of kinetics of the folding process. Such studies provide information about the rate of folding process and can indicate the existence of intermediates. The kinetics of protein refolding are examined by first unfolding the protein with heat, denaturant, or by other means followed by rapid change in the experimental conditions to favor the native state. Folding is then followed by monitoring the changes in the values for structural probes as a function of time. Protein unfolding kinetics are measured in the reverse manner. In addition, it has been observed that the rate of folding depends upon the final folding conditions and not upon the conditions used to unfold the protein (Creighton and Goldenberg, 1984).

In the simplest case of folding or unfolding kinetics, a single kinetic phase is observed. If the folding/unfolding amplitude accounts for the entire signal change in the

equilibrium transition (the difference in the signal for the folded minus the unfolded), then no partial folding/unfolding has preceded the rate-limiting step (Schmid, 1993). Such results indicate that partially unfolded intermediates do not accumulate.

Multiphasic kinetics may represent the sum of two or more single exponential processes, a series of different processes in a sequential pathway, or a combination of both. Multiphasic folding kinetics are observed where either the unfolded population of molecules is heterogeneous or if partially folded states are populated along the folding pathway.

To determine the mechanism and pathway of unfolding and refolding, any intermediates that define and direct the pathway must be identified. In case of pure kinetic controlled folding, the population of intermediates is governed by the activation free energy between the individual intermediates. These intermediates may be unstable at equilibrium but might be detectable as transient kinetic intermediates. If the kinetics associated with the folding to the final state involve a lag phase, then the process must be sequentially coupled to an earlier process. In such cases, all the steps preceding this step are rapid and are not observed directly.

1.7 Background and Significance

As noted earlier, the relative importance of hydrogen bonding and the hydrophobic effect in the stabilization of proteins is the subject of considerable controversy. This laboratory has addressed this issue by examining the denaturation of RNase A with denaturants that differ in their ability to hydrogen bond. The general idea is that

denaturants with a lesser ability to hydrogen bond should destabilize RNase A or any other protein to a lesser degree than those with a greater ability to hydrogen bond if hydrogen bonding is a major contributor to the stability. Hence, higher concentrations of the former would be required to denature the protein. In addition, comparison of the denaturants that incrementally differ in the ability to hydrogen bond will allow for a quantitation of this effect.

Ghuman et al. (Ghuman, R., Henriquez, V. and Biringer, R. G., unpublished data) have examined the denaturation of RNase A by a number of different alkylureas. The data (Figure 5) show that the concentration of 1,3-dimethylurea required to denature RNase A is higher than that for N-methylurea and the concentration of N-methylurea required to denature RNase A is higher than that for urea. Since 1,3-dimethylurea has one less hydrogen available to hydrogen bond than does N-methylurea and two less hydrogens than urea, clearly, hydrogen bonding must be an important contributor to the stability of this protein. Further, for these denaturants, hydrogen bonding appears to dominate over the hydrophobic effect, as both N-methylurea and 1,3-dimethylurea are more hydrophobic than urea. In contrast, the data for tetramethylurea and ethylurea are similar to urea even though they have a reduced ability to hydrogen bond; tetramethylurea has no hydrogens available to hydrogen bond and ethylurea has one less hydrogen than urea. However, these denaturants are significantly more hydrophobic than the other denaturants indicating that the hydrophobic effect also contributes to the stability of this protein.

In order to extract the hydrogen bonding component from this data, the hydrophobic effect must be subtracted out. This requires knowledge of the incremental

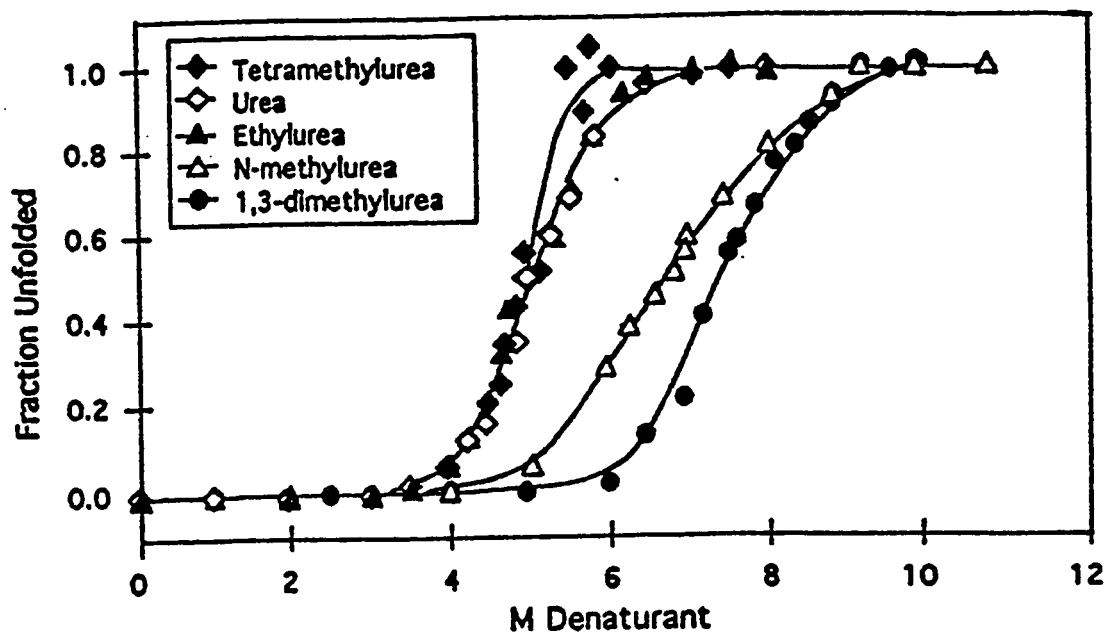


Figure 5: Alkylurea studies. Denaturation profile of RNase A using a variety of alkylureas at pH* 4.00 and 17 °C as monitored by the intrinsic fluorescence (280/305 nm). Raw data was standardized by conversion to fraction of unfolded molecules. Reproduced with permission from Ghuman, R.; Henriquez, V; Biringer, R. G. unpublished data.

effect of increasing denaturant hydrophobicity on the stability of RNase A. In order to establish this relationship, we plan to examine the concentration mediated denaturation of RNase A by a series of monohydric alcohols that differ incrementally in their extent of hydrophobicity.

The effect of monohydric alcohols on the stability of RNase A and other proteins has been reported previously (Schrier et al. 1965; Brandts and Hunt, 1967; Biringer and Fink, 1982). Very few studies have examined the complete concentration mediated unfolding of proteins or peptides at fixed temperatures. None of these involved RNase A. However, results from thermal denaturation of RNase A in the presence of low alcohol concentrations (Schrier et al. 1965; Brandts and Hunt 1967) indicates that the range of hydrophobicities for the soluble alcohols should be large enough to provide useful information.

This study may also provide insight regarding the mechanism of denaturation and the production and stabilization of partially folded intermediate states. Several studies have shown that weak denaturants such as aqueous/methanol solvent systems can serve to populate intermediate states (Biringer and Fink, 1982; Lustig and Fink, 1992). It is thought that alcohol cosolvents stabilize partially-folded states relative to both native and unfolded states which results in an increased concentration of the intermediate structures.

1.8 RNase A as a Model for Protein Folding

To accomplish the goals of this project, RNase A was used as a model protein. RNase A is a small, globular protein that catalyzes the hydrolysis of ribonucleic acid. The

protein has been studied extensively and consists of a single polypeptide chain of 124 amino acid residues with four disulfide linkages, four prolines, and six tyrosines. X-ray crystallography reveals that three of the tyrosine residues (Tyr-115, -76, and -73) are solvent exposed in the native structure while the other three tyrosines are located in the hydrophobic core of the protein. The enzyme undergoes reversible unfolding without loss of catalytic activity. RNase A is a very hydrophilic protein and tends not to aggregate even in the unfolded state. Thus, RNase A serves as an excellent model compound to investigate the mechanism of protein folding.

2. MATERIALS AND METHODS

2.1 Materials

Bovine pancreatic Ribonuclease A and ultra pure guanidinium chloride were purchased from Sigma Chemical Company, St. Louis, MO. Bromocresol green and 2,6-dinitrophenol (DNP) were purchased from Aldrich. The alcohols, methanol, 1-propanol, and 2-propanol were purchased from Fisher and were HPLC grade.

2.2 Purification of RNase A

RNase A was purified further on a Sephadex SPS-25 ion-exchange column (1.5 X 25 cm) using 0.15 M phosphate buffer at pH 6.5 as the eluent (Biringer and Fink, 1982). For a typical purification process, 150 mg of RNase A was dissolved in 1-2 mL of the eluting buffer and loaded on to a preequilibrated column and then eluted at room temperature. This procedure facilitates the separation of aggregated material and RNase S from monomeric RNase A. The pure monomeric fractions of RNase A were pooled and dialyzed against 20 L of deionized-distilled water for 24 hours in the cold room. Dialysis was repeated twice more. The dialyzed product was frozen and then lyophilized and stored at -20 °C.

2.3 Determination of $p_{a_{H^+}}$ for Aqueous / Alcohol solutions by the Indicator Method

The effective proton concentration in dilute solutions can be measured with a pH meter. In aqueous solutions containing other protic solvents (e.g. alcohols), the effective proton concentration (protonic activity, where $-\log [\text{protonic activity}] = p_{a_{H^+}}$) will differ

from that which is measured with a pH meter. This is due to the fact that protic solvents contribute significantly to the hydrogen ion equilibria and the pH electrode contains only aqueous reference solution. Further, the contribution is dependent on the cosolvent concentration. Since the conformation and denaturation of proteins are pH dependent, it is imperative that all solutions used in an experiment have the same $p_{a_{H^+}}$. Fortunately, methods have been developed that allow the precise determination of protonic activities in solutions that contain protic solvents other than water.

The $p_{a_{H^+}}$ of aqueous/alcohol solutions were determined by the indicator method as outlined by Douzou (1977). In general, the indicator must have distinct spectral bands for both the protonated and the deprotonated forms. The best indicator is the one that has a pK close to the pH of interest. In our experiments, it was found that bromocresol green and 2,6-dinitrophenol (DNP) were appropriate for $p_{a_{H^+}}$ 4.00 and 3.00 respectively. First, aqueous standard curves were established to provide a spectroscopic measure of protonic activity. The spectra of each indicator was measured in aqueous buffer as a function of pH. In dilute aqueous solution the following holds true

$$pH = pH^* = p_{a_{H^+}}$$

where pH^* is the pH measured with the pH meter. Next, the $p_{a_{H^+}}$ of aqueous/alcohol solutions were determined by comparison of the absorbance spectrum for the indicator in the particular aqueous/alcohol solution to those from the aqueous standard curve.

2.4 Aqueous Standard Curve

An aqueous standard curve was established for the bromocresol green indicator. A 500- μ L aliquot of indicator stock solution at a concentration of 1 mg/mL was added to a

50-mL volumetric flask and diluted to the mark with 0.05 M acetic acid. The solution was mixed by inverting the flask several times. The diluted indicator solution was carefully titrated to pH 2.0 using small quantities of 1 M HCl. A 3.00-mL aliquot of solution was removed and placed into a clean test tube. The remaining solution was titrated to pH 3.2 with 1 M NaOH and another 3.00 mL was removed and placed into a clean test tube. The same procedure was repeated until the solutions with pH values of 2.0, 3.2, 3.4, 3.6, 3.8, 4.0, 4.2, 4.4, 4.6, 4.8, 5.0, 6.0 were prepared.

The absorbance spectra for each of these solutions was measured. At pH 2.00, 100% of the protonated form of the indicator is present and 100% deprotonated form is present at pH 6.00. Examination of the pH 2.00 and pH 6.00 samples revealed that the λ_{max} (wavelength of the maximal absorbance) for the protonated and deprotonated forms were at 446 and 616 nm respectively. The absorbance spectra for all other solutions were taken and the absorbance at 446 nm and 616 nm recorded. Since the absorbance at 616 nm is proportional to the concentration of the deprotonated form and the absorbance at 446 nm is proportional to the concentration of the protonated form, then the ratio of the absorbances at these wavelengths (R_e), A_{616} / A_{446} , is a measure of the ratio of the concentration of these species in the particular solution. Further, since the concentration ratio and hence the absorbance ratio is a function of pH, (equation 7) then R_e serves as a spectroscopic measure of pH.

$$\text{pH} = \text{pK} + \log \left(\frac{[\text{deprotonated}]}{[\text{protonated}]} \right) = \text{pK} + \log R_e \quad (7)$$

R_e values were calculated for each solution and plots of R_e vs. pH and $\log R_e$ vs pH were

prepared to serve as standard curves.

A standard curve was prepared for 2,6-dinitrophenol in a similar manner. In this case, the solutions were prepared with 0.05 M formic acid. The λ_{max} for the protonated and deprotonated were found to be 348 nm and 430 nm respectively, and Re values were calculated as ratio of the absorbance at these wavelengths (A_{430}/A_{348}).

2.5 Determination of p_{aH^+} in Aqueous/Alcohol Solutions

The molarity of the pure monohydric alcohols, methanol (24.7 M), 1-propanol (13.37 M) and 2-propanol (13.06 M) were determined by their density and molecular weight. An appropriate volume of an aqueous/alcohol stock solution at 90-95% of the maximum concentration was prepared for each alcohol and made 0.05 M in acetic acid. A 10- μL aliquot of the bromocresol green stock solution was added to 1990 μL of the alcohol solution and placed into a spectrophotometer cell and then scanned. The absorbances at λ_{max} for both the protonated and deprotonated forms of the indicator were used to calculate the initial Re. Based on the aqueous standard curve, either 1 M HCl or 1 M NaOH was added until an Re value corresponding to the desired p_{aH^+} (4.00) was obtained. The pH of the solution was then measured directly with a pH meter (pH^*). The p_{aH^+} for the remaining stock solution was adjusted to the desired value by titrating to this pH^* . Solutions at p_{aH^+} 3.00 were prepared in a similar manner using 2,6-dinitrophenol and 0.05 M formic acid as noted above.

2.6 Examination of Protocols for Preparation of Alcohol Dilution Series:

Stock solutions of aqueous and aqueous/alcohol solvent were prepared at p_{aH^+} of

4.00 (0.05M acetate) by methods noted above. A dilution series was prepared for alcohol concentrations from 0 M to the highest M solution in 1 M increments by mixing appropriate volumes of the two solutions. A 1990- μL aliquot of each alcohol concentration was placed in a 3-mL spectrophotometer cell and scanned as a blank. To this, 10 μL of indicator stock solution was added, the solution was mixed and then scanned. The initial $\text{p}a_{\text{H}^+}$ was determined by measuring the absorbances at the appropriate wavelengths. The sample was titrated until the correct Re value was obtained and then the final pH^* measured with a pH meter.

The results were examined by plotting : 1) the initial $\text{p}a_{\text{H}^+}$ vs M denaturant, and 2) final pH^* vs M alcohol. For all the alcohols under study, the initial $\text{p}a_{\text{H}^+}$ vs M denaturant plot was not linear indicating that solutions in the dilution series must be adjusted individually. The final pH^* vs M alcohol plot gave the pH^* value to which the unit M solutions must be adjusted. These experiments were also performed for a $\text{p}a_{\text{H}^+}$ of 3.00 and similar results were obtained.

2.7 Preparation of Protein Stock Solutions

The purified protein was dissolved in the appropriate 0.05 M buffer to a concentration of 5 mg/mL. The protein solution was mixed slowly by magnetic stirring to prevent frothing and then filtered through a 0.45 μm teflon membrane to remove dust. The protein concentration was checked spectrophotometrically. A 50- μL aliquot of the stock protein solution was added to 800 μL of aqueous 0.1 M acetate buffer at pH 6.00. The absorbance was measured at 278 nm after stirring with a hand-held stirrer. The protein

stock solution concentration was calculated from this value (MW : 13,800; ϵ_{278} : 9800 AU/M cm) (Sage and Singer, 1962).

2.8 Preparation of Alcohol Dilution Series

In all experiments, the alcohol dilution series was prepared from one concentrated alcohol stock solution and the corresponding aqueous buffer. Since the plot of initial pH* vs M alcohol was not linear, all the unit molar solutions for the dilution series were adjusted to the correct $p_{a_{H^+}}$ individually. The high molar alcohol solution was prepared in the appropriate buffer and adjusted to the correct $p_{a_{H^+}}$ according to the standard curve. Appropriate volumes of aqueous buffer (0.05 M acetate or 0.05 M formate) and concentrated alcohol stock solutions were mixed to give a total volume of 16 mL. The final alcohol concentrations were chosen such that they would correspond to unit molar concentrations after addition of the stock protein solution. Each vial was capped and mixed several times followed by vigorous vortex mixing. The pH* of each solution was adjusted carefully with a pH meter, to the appropriate value for the particular $p_{a_{H^+}}$. The half molar concentrations were prepared by mixing 8.00 mL of adjacent unit molar concentrations prepared in the previous step. The pH* of these solutions were measured and the $p_{a_{H^+}}$ checked through intrapolation of the pH* versus M alcohol graph. The corresponding quarter molar concentrations were prepared by mixing 4.00 mL of adjacent unit molar and half molar concentrations.

Three samples were prepared for each alcohol concentration. Into each of the three labeled test tubes, 1900- μ L aliquots of each alcohol solution were added. A 100- μ L

aliquot of concentrated protein stock solution was added to two of the three tubes and 100 μL of the aqueous buffer was added to the third set. The latter sets served as blanks. Each test tube was stoppered with a polypropylene stopper and mixed by inverting the tube several times followed by vigorous vortex mixing. The final concentration of the protein after addition to the particular alcohol solution was 18 μM . The solutions were allowed to equilibrate at room temperature for 30 minutes prior to taking any measurements. This procedure was followed to allow the protein to unfold to an equilibrium population of molecules. Fluorescence and CD measurements for each particular set of conditions were performed with the same set of solutions.

2.9 Fluorescence-Monitored Chemically-Induced Denaturation Transitions

All fluorescence measurements were performed with a Perkin Elmer LS-3 fluorometer. The cuvet cooling block was equilibrated to 17 ± 0.1 $^{\circ}\text{C}$. Temperature was monitored with a digital thermometer by placing the probe directly into the cuvet. The excitation and the emission wavelengths were set to 280 and 305 nm respectively. The solutions were precooled in a chilled water bath to a temperature of 17 ± 0.1 $^{\circ}\text{C}$ prior to taking the measurements. The fluorometer was “auto-zeroed” against the appropriate blank buffer and the fluorescence of the samples was measured directly. After each measurement, all of the sample was removed from the cuvet with a pasteur pipet and the next solution added. Replicate solutions were measured in a back-to-back fashion. The amount of cross contamination was kept to a minimum by measuring the fluorescence in order of increasing alcohol concentration. The same procedure was followed for all the

denaturants at both p_{H} 3.00 and 4.00.

To determine the extent of unfolding for each set of conditions, the fluorescence of the protein denatured in guanidinium chloride solution (GdmCl) was examined. The solution was prepared by dissolving the appropriate amount of GdmCl in distilled deionized water. Into each of three test tubes, 1900- μL aliquots of 6 M GdmCl were carefully pipetted out. A 100- μL aliquot of concentrated protein solution was added to two of the tubes and 100 μL of aqueous buffer was added to the third tube. Each test tube was stoppered with a polypropylene stopper and mixed by inverting the tube several times followed by vortex mixing. The final concentration of the GdmCl was 5.7 M in each case. This concentration has been shown to completely denature the RNase A (Santoro and Bolen, 1988). The solutions containing proteins were allowed to equilibrate at room temperature for 30 minutes prior to taking any measurements.

2.10 CD-Monitored Chemically-Induced Denaturation Transitions

2.10.1. General Method

The far UV-CD measurements were carried out on a Cary 61 Spectropolarimeter. The CD instrument was purged with dry nitrogen at all times. All the measurements were made with a 1.00-mm path length cylindrical CD cell. The temperature of the cylindrical cell holder was adjusted to 17 ± 0.1 °C and was monitored with a digital thermometer. The CD measurements for a particular set of conditions were performed with the same solutions that were used for the fluorescence measurements. The solutions were precooled in a chilled water bath set to 17 ± 0.1 °C. After temperature equilibration for 8-10 minutes

in the cylindrical cell holder, each solution was scanned on the 0.02 deg scale from 260 nm to 218 nm. Replicate solutions were measured in a back-to-back fashion. The data was averaged for two simultaneous scans of the same sample. The blank solutions were scanned and the results subtracted from the appropriate sample spectra. The ellipticity at 222 nm was compiled for each set of solvent conditions and analyzed. The amplitude at this wavelength corresponds primarily to the α -helix structure.

2.10.2. Singular Value Decomposition (SVD) Analysis Measurements

Singular value decomposition (SVD) analysis is a matrix algebra technique that is used to simultaneously solve a complex mathematical function in terms of the individual mathematical expressions that make up the complex function. This technique has been used by Compton and Johnson (1986) to evaluate the CD spectra in terms of the contributions from the five basic contributors to the spectrum: α -helix, β -parallel sheet, β -antiparallel sheet, turn, and other structure. The technique employs empirically-derived spectra (basis sets) for each of the secondary structures and simultaneously fits them to a protein CD spectra. The percentage contribution of each secondary structure to the protein CD spectrum is obtained from the analysis.

Spectra in this study were evaluated using the 184 nm basis sets derived by Compton and Johnson (1986). These allow for the evaluation of CD spectra taken from 260 nm to 184 nm. Excel™ (Microsoft) was used to perform the mathematical manipulations.

SVD analysis for RNase A in methanol at p_{H^+} 3.00 was carried out for solutions

in the 16-23 M range. The solutions were scanned in 0.2-mm path length cell from 260 nm to 200 nm. The high dynode voltage at wavelengths lower than 200 nm was too large to yield usable data. To obtain data below 200 nm, the same solution was scanned using a 0.05-mm path length cell from 200 nm or 184 nm. The same sample was scanned twice as noted above and the average results used in the analysis. All data were converted to the 0.02-deg scale.

2.10.3. 10-Camphor Sulfonic Acid (CSA) Standardization for SVD Measurements

The amplitude of the CD signal obtained from all experiments were converted to $\Delta\epsilon$ units by standardization against 10-camphor sulfonic acid prior to data analysis. Scaling is performed by multiplying each data point by a scaling factor (SF). The scaling factor is calculated as follows:

$$SF = \left(\frac{\Delta\epsilon_{290.5 \text{ CSA}}}{\theta_{290.5 \text{ CSA}}} \right) \left(\frac{A_{285 \text{ CSA}}}{\epsilon_{285 \text{ CSA}}} \right) \left(\frac{9800 \text{ AU/M}\cdot\text{cm}}{A_{278 \text{ RNaseA}}} \right) \left(\frac{1}{124 \text{ residues}} \right) \quad (8)$$

where $\Delta\epsilon_{290.5 \text{ CSA}}$ is the molar ellipticity in $\Delta\epsilon$ units for CSA at 290.5 nm, $\theta_{290.5 \text{ CSA}}$ is the measured ellipticity (chart divisions) for the CSA standard at 290.5 nm, A_{285} is the absorbance of the CSA standard at 285 nm, ϵ_{285} is the molar extinction for CSA at 285 nm, 9800 AU/M·cm is the molar extinction for RNase A at 278 nm, A_{278} is the absorbance of the RNase A solution at 278 nm, and 124 residues is the number of amino acid residues in RNase A. The literature values of +2.36 and 34.5 AU/M·cm were used for $\Delta\epsilon_{290.5 \text{ CSA}}$ and $\theta_{290.5 \text{ CSA}}$ respectively. The computation requires that the absorbance of the protein and CSA be measured in cells with identical path lengths at the same concentrations used

in absorbance measurements (Labhardt, 1980).

A 0.7% (w/v) CSA standard was prepared in distilled deionized water. The absorbance of CSA was measured at 285 nm. The CSA standard solution was placed in a 0.2-mm path length cell and scanned at the rate of 0.2 nm/sec using 0.20-deg scale at 17 ± 0.1 °C. Baseline adjustments were carried out using deionized-distilled water as the blank. Both the sample (0.7% CSA) and water blank were scanned from 350 nm to the lowest possible wavelength (184 nm). The ellipticity and absorbances were used to calculate the scaling factor using equation 8.

2.11 Data Analysis

Two methods have been used to analyze the denaturation transitions, linear extrapolation and least-squares fitting. Arguments presented by Pace et al. (1990) and Schellman (1978) indicate that the linear extrapolation method is appropriate for urea-induced unfolding transitions but may not be appropriate for other denaturants.

The linear extrapolation method requires that all data sets be standardized by conversion of the raw amplitude data to the fraction of unfolded molecules (F_u) present by the following relation:

$$F_u = (y_D - y) / ((y_D - y) + (y - y_N)) = (y_D - y) / (y_D + y_N) \quad (9)$$

where y is the signal amplitude (e.g., fluorescence) observed within the unfolding transition and y_N and y_D are the characteristic signal amplitudes for the native and denatured states respectively at the molarity of the denaturant where y is measured.

Figure 6A shows the raw fluorescence data for a typical urea-mediated

denaturation of RNase A. Values for y_N and y_D within the transition region are obtained through a linear least squares extrapolation of the pretransition and posttransition regions respectively and the raw data is converted to units of fraction of unfolded molecules F_u with equation 9 (Figure 6B).

Free energies of unfolding, ΔG , are calculated for each point in the transition region by the following relationship:

$$\Delta G = -RT \ln F_u \quad (10)$$

This assumes that each individual transition approximates a two-state situation. Plots of ΔG versus denaturant concentration within the transition regions are analyzed by linear regression analysis using the relationship:

$$\Delta G = \Delta G^{\circ} - m \times [\text{denaturant}] \quad (11)$$

where ΔG° is the free energy change in the absence of denaturant in any particular solvent system and m is the slope of the straight line and thus a measure of the dependence of ΔG on the denaturant concentration. Figure 7 shows that ΔG calculated using equation 9 varies linearly with urea concentration. This indicates that folding is a cooperative phenomenon and follows the two-state model. In all cases, only data with ΔG in the ± 1.5 kcal/mol range should be employed in the linear regression analysis, as the error is minimal in this range.

At the transition midpoint, ΔG is zero, as the concentration of the unfolded and native species are equal. At this point, equation 11 reduces to:

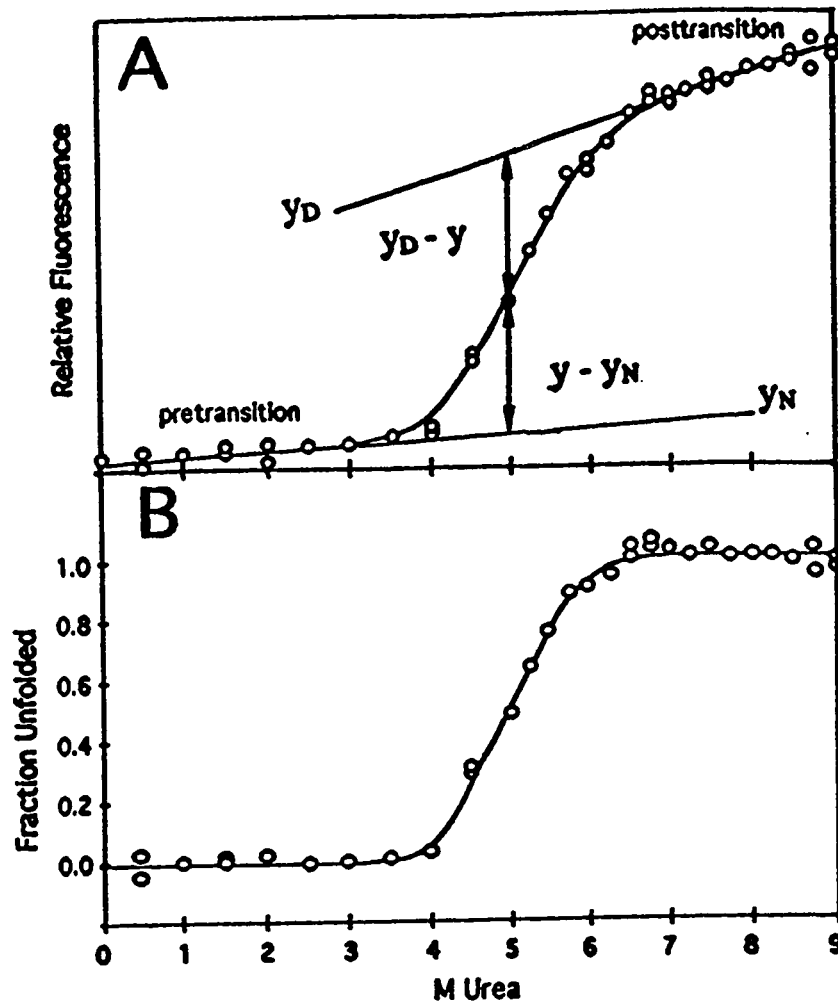


Figure 6: Data analysis. (A) Raw data for the fluorescence-monitored urea-mediated unfolding of RNase A (pH 4.0, 17 °C). The straight lines extrapolated from the pre and post transition regions are used to obtain Y_N and Y_D in the transition region. (B) Standard denaturation profile for a plot of fraction of unfolded molecules (F_u) vs M urea. The raw data given in A was standardized to units of F_u by using equation 9.

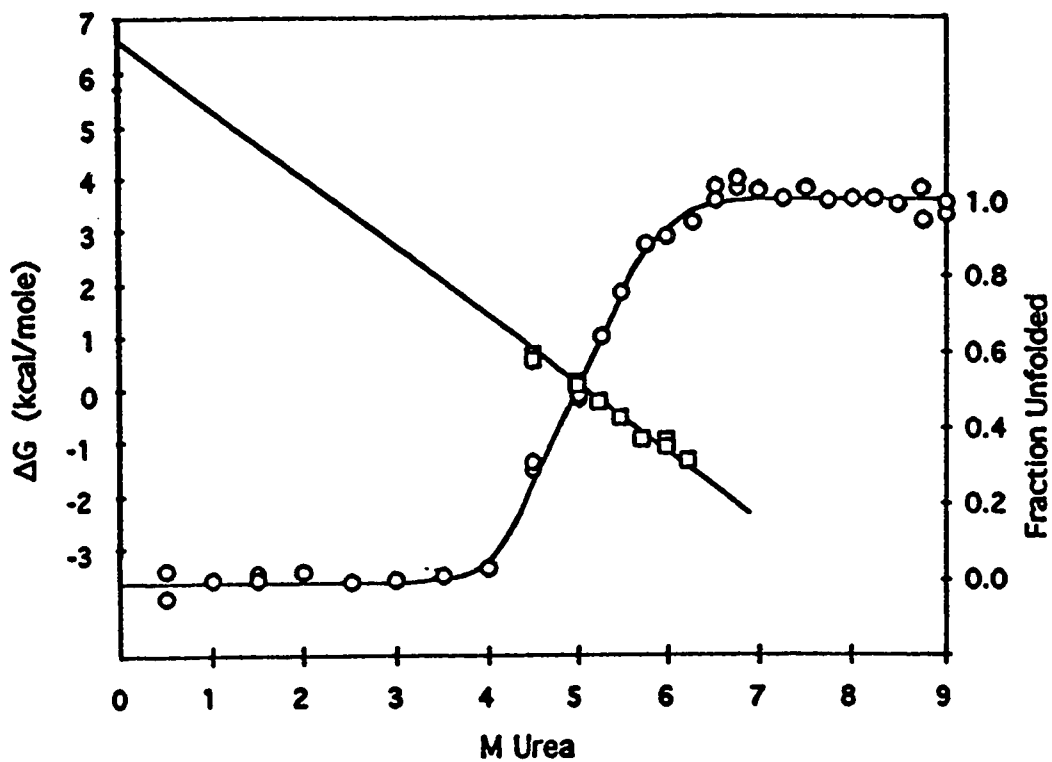


Figure 7: Free energy vs F_u curve. ΔG vs M urea and F_u vs M urea for the fluorescence-monitored urea unfolding of RNase A. The linear relationship of ΔG suggests folding is a cooperative phenomenon following the two-state model.

$$0 = \Delta G^{50} - m \times C_m \quad (12)$$

or

$$C_m = \Delta G^{50} / m \quad (13)$$

where C_m is the concentration of the denaturant which corresponds to the transition midpoint. The C_m value for each transition is calculated from equation 13. All fluorescence data and the $p_{a_{H^+}}$ 4.00 CD data obtained in this study were evaluated by this method. As discussed in the results section, posttransition baselines could not be obtained. For this reason, the fluorescence and CD amplitudes for RNase A denatured in 5.7 M GdmCl were used for the respective y_D values. Excel™ (Microsoft) was used to perform all linear regression analyses and C_m calculations.

Santoro and Bolen (1988) have shown that the linear extrapolation method underestimates ΔG^{50} for GdmCl denaturation curves and that a nonlinear least squares fit is more appropriate. In light of this, all data was also analyzed by this method. Analysis of the data involves the nonlinear least-squares fitting of the raw data to the equation (Santoro and Bolen, 1988; Pace et al. 1990):

$$y = \frac{\{y_f + m_f [D]\} + \{y_u + m_u [D]\} (\exp\{-\Delta G_D^0 - m[D]/RT\})}{\{1 + \exp\{-\Delta G_D^0 - m[D]/RT\}\}} \quad (14)$$

where y_f and m_f represent the intercept and slope of the pretransition baseline, y_u and m_u represent the intercept and slope of the posttransition baseline, $[D]$ is the molarity of the denaturant, m is the dependence of the ΔG on the denaturant concentration, ΔG_D^0 is ΔG at

zero denaturant concentration, and R and T have their usual meaning. Data were fitted to this expression with NFITTM a nonlinear least-squares analysis package (Island ProductsTM, Galveston, Texas).

2.12 Evaluation of the Thermodynamic Parameters

The two parameters used to characterize denaturation transitions are the C_m and the m value. The C_m is complex in that it depends on both the stability of the protein in the absence of denaturant (ΔG°) and the value of m (equation 13). The larger the value of C_m , the more stable the protein. The value of m measures the dependence of the free energy of denaturation on denaturant concentration. The value of m provides a quantitative measure of the effect of denaturant on protein structure (Pace and Marshall, 1980). For processes which adhere to the two-state model, Tanford (1968) has shown that the value of m is directly related to degree denaturant binding to the regions of the protein that are newly exposed by the denaturation process. The higher the absolute value of m , the more significant is the interaction. Schellman (1978), on the other hand, has shown that the value of m is also a measure of the difference between the solvent exposed surfaces areas of the denatured and native states. Here, large absolute values of m correspond to highly unfolded denatured states.

3.0 RESULTS

3.1 Protonic Activity for Aqueous/Alcohol Solutions by the Indicator Method

It is well established that the stability of RNase A and other proteins is strongly affected by the pH (Pace et al. 1990). As a result, it is paramount that the actual protonic activity pa_{H^+} of all solutions be identical for a given experiment. We have adopted the indicator method to determine the pH^* necessary to achieve the desired protonic activity (pa_{H^+}) (Douzou, 1977). The pa_{H^+} of aqueous/organic solutions were determined by measuring the relative absorbance amplitudes of the protonated and the deprotonated spectral curves in the particular solvent system and comparing the values to the aqueous standard curve. Figures 8 and 9 show the plots for the aqueous standard curves obtained with 2,6-dinitrophenol and bromocresol green respectively. Linear regression analysis of the linear region of each plot was used to determine the correct log Re necessary for adjusting the solutions to correct pa_{H^+} .

The Re values obtained from absorbance spectra were used to determine the protonic activity of unit molar alcohol solutions prepared by mixing appropriately buffered aqueous and concentrated alcohol solutions. It was found that this method produced solutions with protonic activities that differed significantly from the desired value for all solvent systems examined, indicating that each solution must be adjusted individually. To facilitate this, a pH^* vs M alcohol standard curve was developed for each set of experimental conditions. Unit molar alcohol solutions containing the appropriate indicator were adjusted to the desired pa_{H^+} (3.00 or 4.00) using the spectrophotometric method

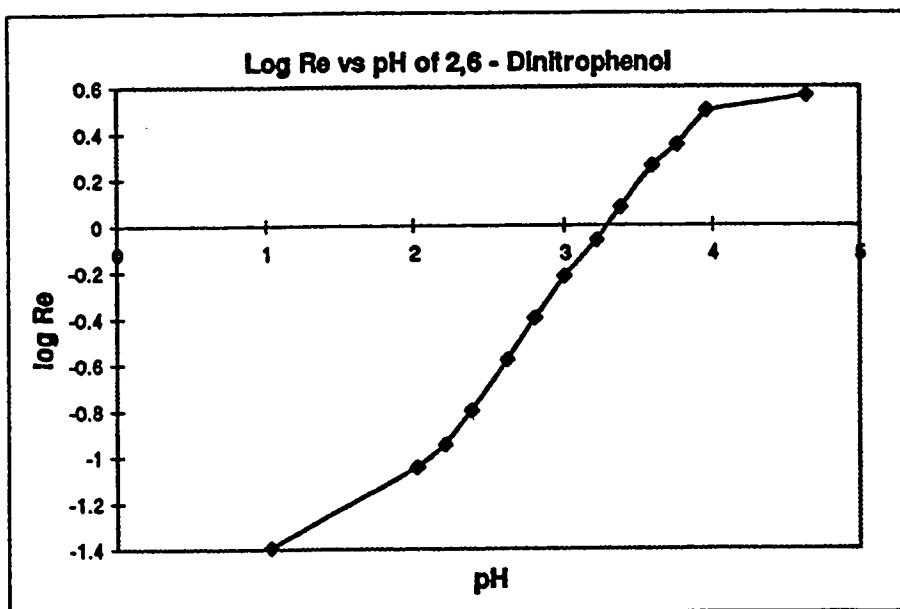


Figure 8: Aqueous standard curve at pH 3.00. Plot of log Re versus pH for the aqueous standard curve at pH 3.00 with 2,6-dinitrophenol as the indicator.

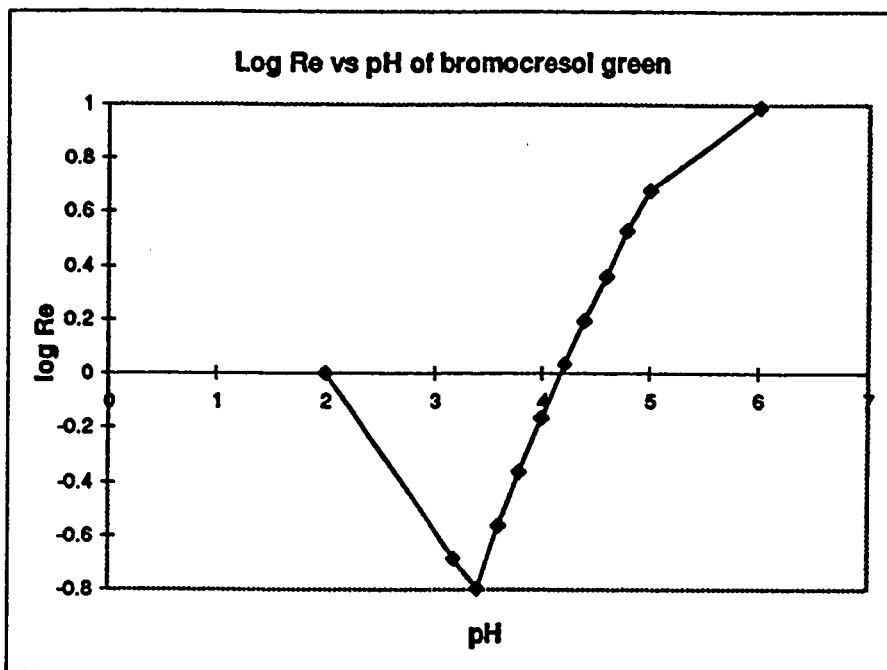


Figure 9: Aqueous standard curve at pH 4.00. Plot of log Re versus pH for the aqueous standard curve at pH 4.00 with bromocresol green as the indicator.

outlined above and the pH measured directly with a pH meter (pH*). Figures 10, 11, and 12 show the final pH* vs M alcohol plot for methanol, 1-propanol and 2-propanol to achieve both $p_{a_{H^+}}$ 3.00 and 4.00. The results obtained from the plots of pH* vs M alcohol, gives the pH* values to which the unit molar alcohol solutions need to be adjusted. All of the unit molar solutions used in subsequent work were adjusted to the desired $p_{a_{H^+}}$ in this manner. The intervening solutions were prepared as discussed earlier in section 2.8. By this procedure, we assume that the protonic activity remains fairly constant over this small range of alcohol concentration.

3.2 Denaturation of RNase A by Monohydric Alcohols

The concentration mediated denaturation of RNase A was examined with a series of monohydric alcohols namely, methanol, 1-propanol, and 2-propanol. The unfolding transitions were monitored by intrinsic fluorescence, and far ultraviolet circular dichroism (UV-CD) at 17 ± 0.1 °C with a constant protonic activity of 3.00 and 4.00 using 0.05 M acetate and formate buffers respectively. All the fluorescence measurements were carried out with the excitation and the emission wavelengths of 280 and 305 nm respectively. Changes in the far UV-CD signal at 222 nm was used to characterize the changes in the α -helix content of the protein. Both fluorescence and circular dichroism measurements were performed with the same solutions for each particular set of conditions.

3.2.1. Denaturation of RNase A by Methanol

Figures 13 and 14 show the denaturation of RNase A by methanol as monitored by intrinsic fluorescence and circular dichroism at 17 ± 0.1 °C. At both $p_{a_{H^+}}$ 3.00 and 4.00, an

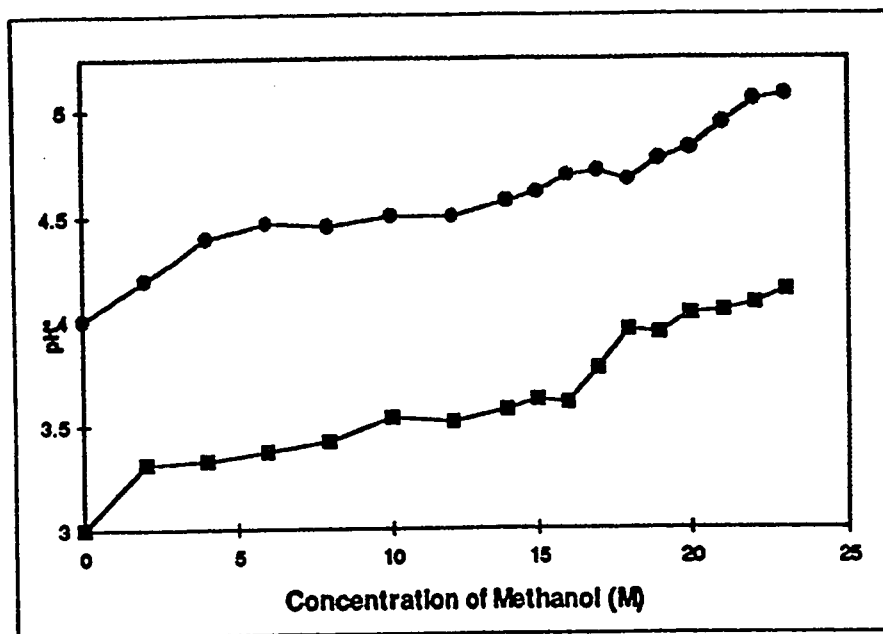


Figure 10: Final pH vs M for methanol. Plot of pH* versus molarity of methanol for $p_{a_{H^+}}$ 3.00 and 4.00. The filled circles (-●-) represent the values obtained at $p_{a_{H^+}}$ 4.00 using bromocresol green while the filled squares (-■-) represent the values obtained at $p_{a_{H^+}}$ 3.00 using 2,6-dinitrophenol as the respective indicators.

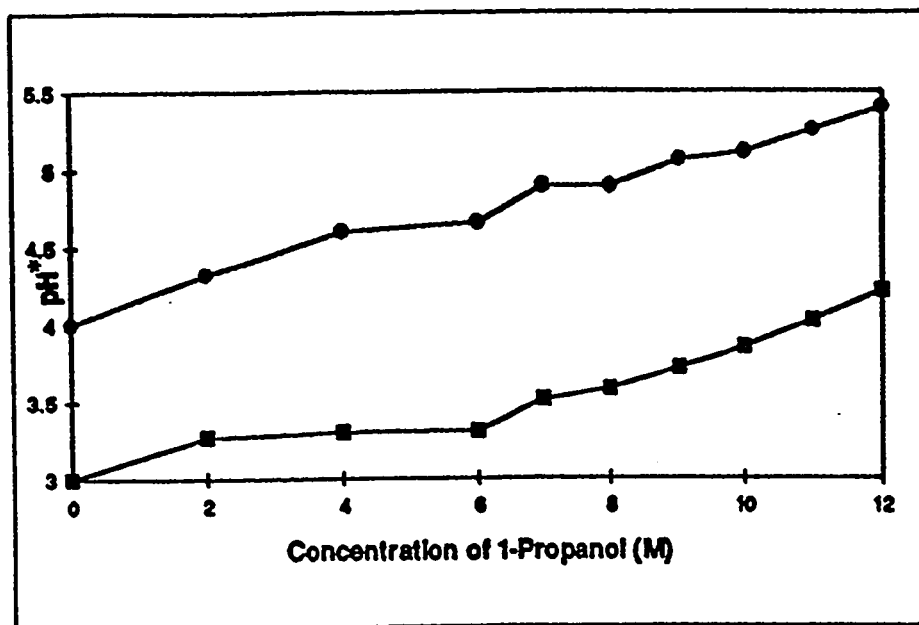


Figure 11: Final pH vs M for 1-propanol. Plot of pH* versus molarity of 1-propanol for $p_{a_{H^+}}$ 3.00 and 4.00. The filled circles (-●-) represent the values obtained at $p_{a_{H^+}}$ 4.00 using bromocresol green while the filled squares (-■-) represent the values obtained at $p_{a_{H^+}}$ 3.00 using 2,6-dinitrophenol as the respective indicators.

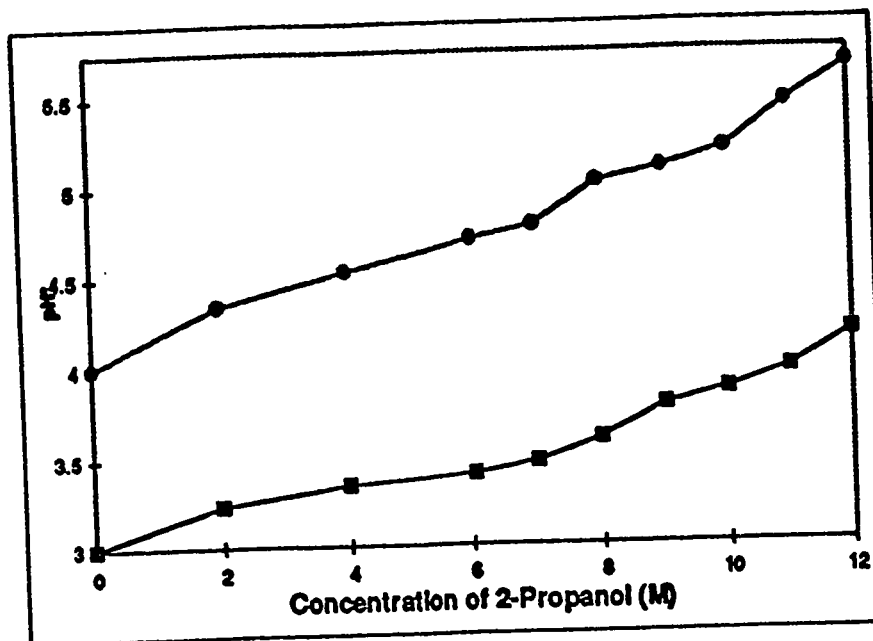


Figure 12: Final pH vs M for 2-propanol. Plot of pH^* versus molarity of 2-propanol for $p_{a_{H^+}}$ 3.00 and 4.00. The filled circles (-●-) represent the values obtained at $p_{a_{H^+}}$ 4.00 using bromocresol green while the filled squares (-■-) represent the values obtained at $p_{a_{H^+}}$ 3.00 using 2,6-dinitrophenol as the respective indicators.

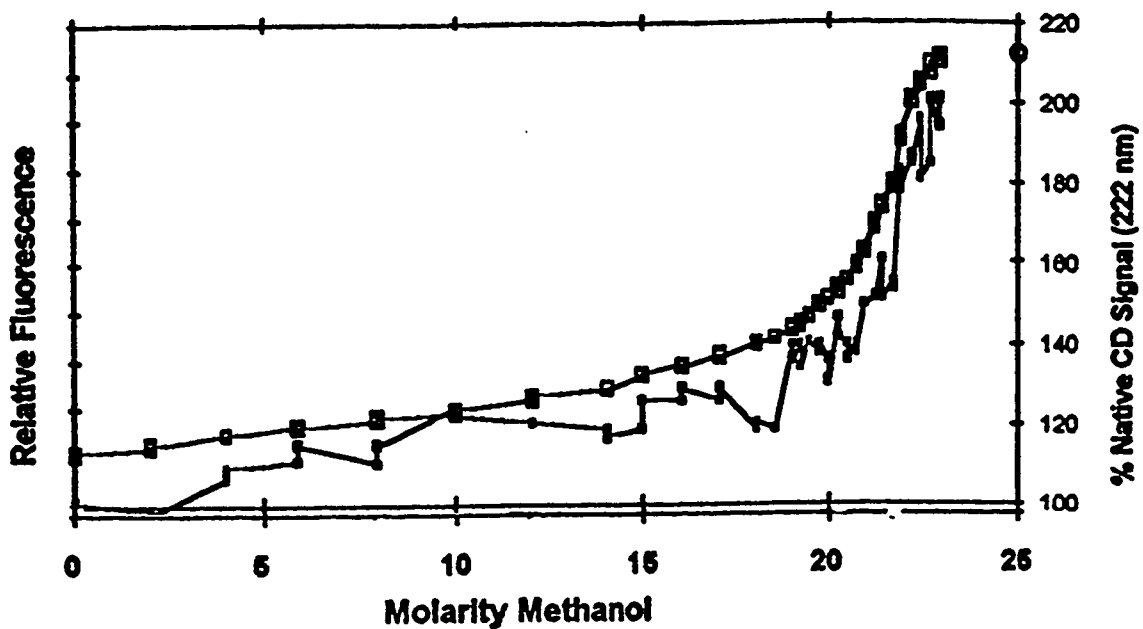


Figure 13: Fluorescence and CD of methanol at $p_{a_{H^+}}$ 3.00. Denaturation of RNase A (18 μ M) by methanol as monitored by intrinsic fluorescence (—○— 280/305 nm) and circular dichroism (CD —■— 222 nm) at $p_{a_{H^+}}$ 3.0, 0.05 M formate buffer and 17 °C. The open circle on the right axis indicates the fluorescence obtained from RNase A denatured in 5.7 M guanidinium chloride at the same temperature and protonic activity.

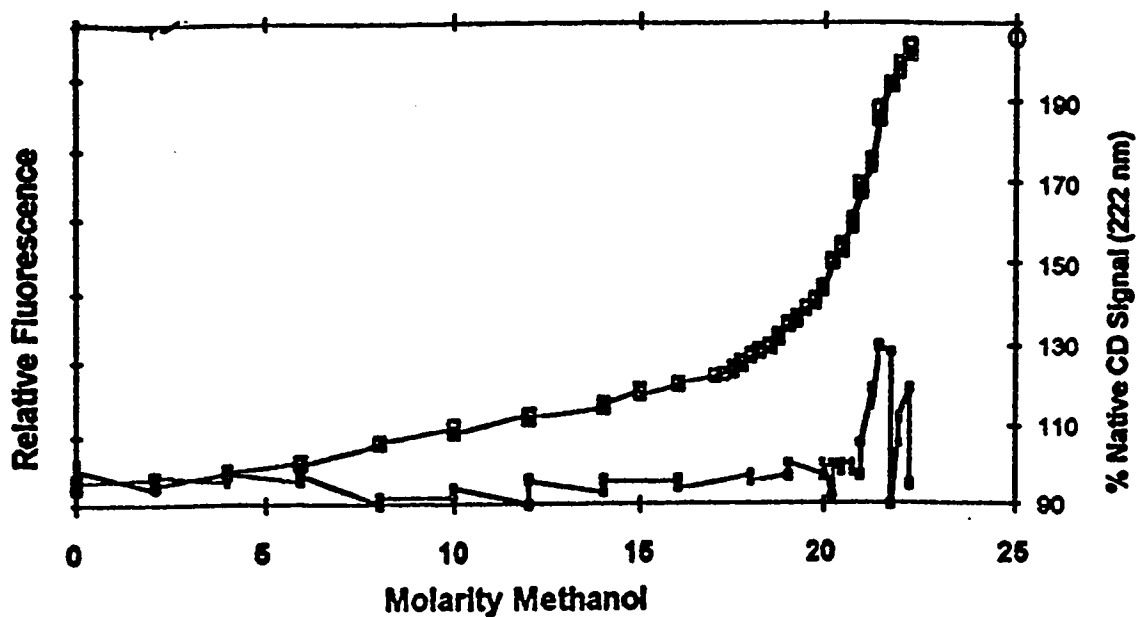


Figure 14: Fluorescence and CD of methanol at $p_{\text{H}} 4.00$. Denaturation of RNase A (18 μM) by methanol as monitored by intrinsic fluorescence (—○— 280/305 nm) and circular dichroism (CD —■— 222 nm) at $p_{\text{H}} 4.0$, 0.05 M acetate buffer and 17 °C. The open circle on the right axis indicates the fluorescence obtained from RNase A denatured in 5.7 M guanidinium chloride at the same temperature and protonic activity.

increase in the fluorescence is observed indicating the loss of tertiary structure. A posttransition baseline could not be obtained for the $p_{a_{H^+}}$ 3.00 data, as the transition region was very close to the maximum concentration of alcohols examined. Higher alcohol concentrations could not be used, because stable pH^* measurements could not be obtained with these solutions. The posttransition baselines for the $p_{a_{H^+}}$ 4.00 data were limited to even lower alcohol concentrations due to protein precipitation. This precipitation problem is discussed in detail in section 3.3. In order to quantitate the extent of unfolding observed, the data was compared to the fluorescence obtained from RNase A denatured in 5.7 M guanidinium chloride. The results show that almost all of the transition was observed.

The unfolding transition for RNase A was also examined via far UV-CD by measuring the ellipticity at 222 nm. The $p_{a_{H^+}}$ 3.00 data (Figure 13) shows an unexpected increase in the CD signal at 222 nm. Comparison to the fluorescence data indicates that an increase in secondary structure accompanies the loss of tertiary structure. The transition midpoints for the CD data were not calculated for $p_{a_{H^+}}$ 3.00, since a posttransition baseline was not obtained and the maximal ellipticity increase is unknown.

In contrast to the methanol-mediated denaturation at $p_{a_{H^+}}$ 3.00, the $p_{a_{H^+}}$ 4.00 data (Figure 14) shows a small increase in ellipticity followed by a small decrease. Comparison to the fluorescence indicates that the loss of tertiary structure does not accompany a corresponding decrease or an increase in secondary structure.

Figure 15 shows the fluorescence-monitored methanol-mediated denaturation data for RNase A at $p_{a_{H^+}}$ 4.00 and 17 ± 0.1 °C in terms of F_u versus M and ΔG vs M . Similar results were obtained from the $p_{a_{H^+}}$ 3.00 data (data not shown). The figure clearly shows a

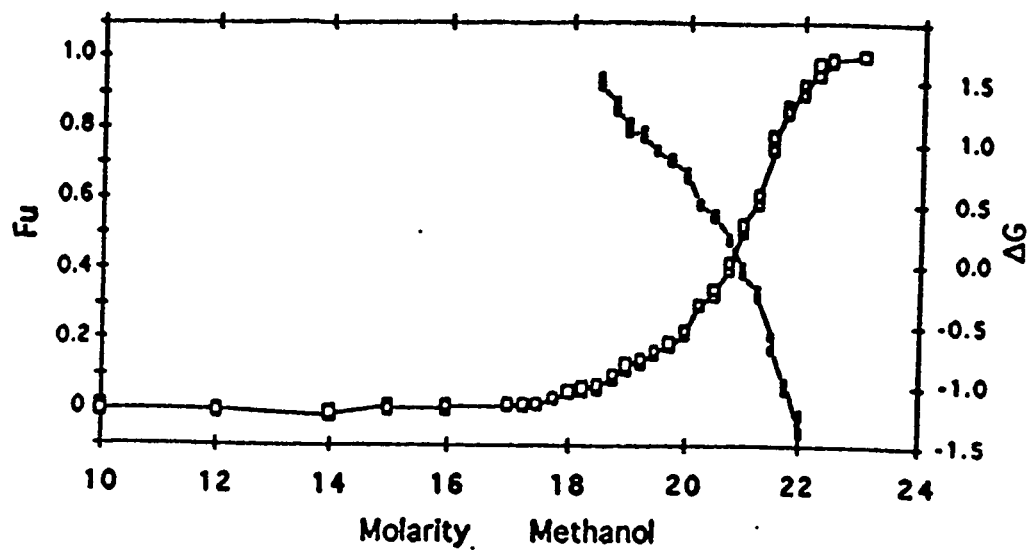


Figure 15: Fluorescence-monitored denaturation of methanol. Fluorescence-monitored denaturation of RNase A (18 μM) by methanol at pH_{H^+} 4.0 and 17 $^{\circ}\text{C}$. Open symbols represent the fraction of unfolded molecules and the filled symbols represent the effect of methanol on ΔG through the denaturation transition. Similar results were obtained for all other experimental conditions.

nonlinear dependence of ΔG on the molarity of the denaturant. As discussed above, such results are characteristic of multistate denaturation transitions and, in such cases, C_m values and m values cannot be calculated. For this reason, C_m values were estimated from the raw data and found to be 21 M for both pH conditions.

3.2.2. Denaturation of RNase A by Propanols

Figures 16 and 17 show the 1-propanol-mediated denaturation profiles of RNase A at p_{H^+} of 3.00 and 4.00. Figures 18 and 19 show the 2-propanol-mediated denaturation profiles of RNase A at p_{H^+} 3.00 and 4.00. Each figure shows the changes as monitored by intrinsic fluorescence and far UV-CD at 17 ± 0.1 °C. For the propanol-mediated denaturations at p_{H^+} 3.00 and 4.00, the relative fluorescence increased with an increase in the alcohol concentration, indicating a net loss in RNase A tertiary structure. A posttransition baseline could not be obtained, as precipitation occurred at the higher propanol concentrations (see section 3.3). In order to quantitate the extent of unfolding observed, the data was compared to the fluorescence obtained from RNase A denatured in 5.7 M guanidinium chloride. The results show that almost the entire transition was observed.

A nonlinear dependence of ΔG on the M 1-propanol and 2-propanol was observed, indicating a multistate transition. For this reason, C_m values were estimated from the data and found to be in the 9-10 M range for both the pH conditions.

The propanol-mediated denaturations at p_{H^+} 4.00 as monitored by far UV-CD are shown in Figures 17 and 19. A decrease in the ellipticity at 222 nm was observed for both

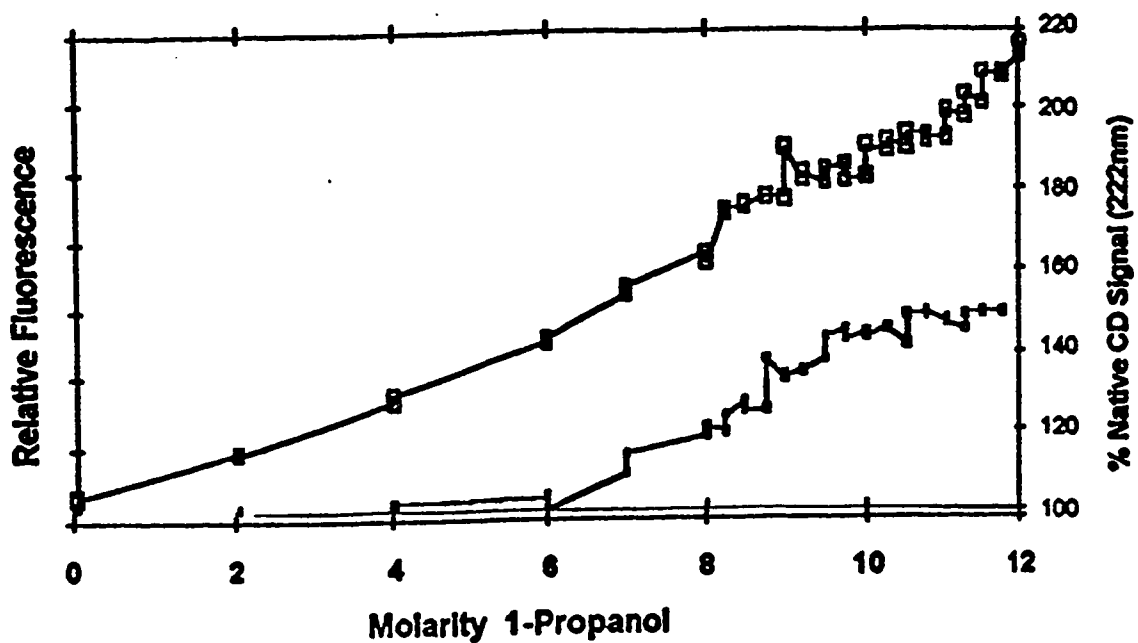


Figure 16: Fluorescence and CD of 1-propanol at p_{H^+} 3.00. Denaturation of RNase A (18 μM) by 1-propanol as monitored by intrinsic fluorescence (—○— 280/305 nm) and circular dichroism (CD —■— 222 nm) at p_{H^+} 3.0, 0.05 M formate buffer and 17 °C. The open circle on the right axis indicates the fluorescence obtained from RNase A denatured in 5.7 M guanidinium chloride at the same temperature and protonic activity.

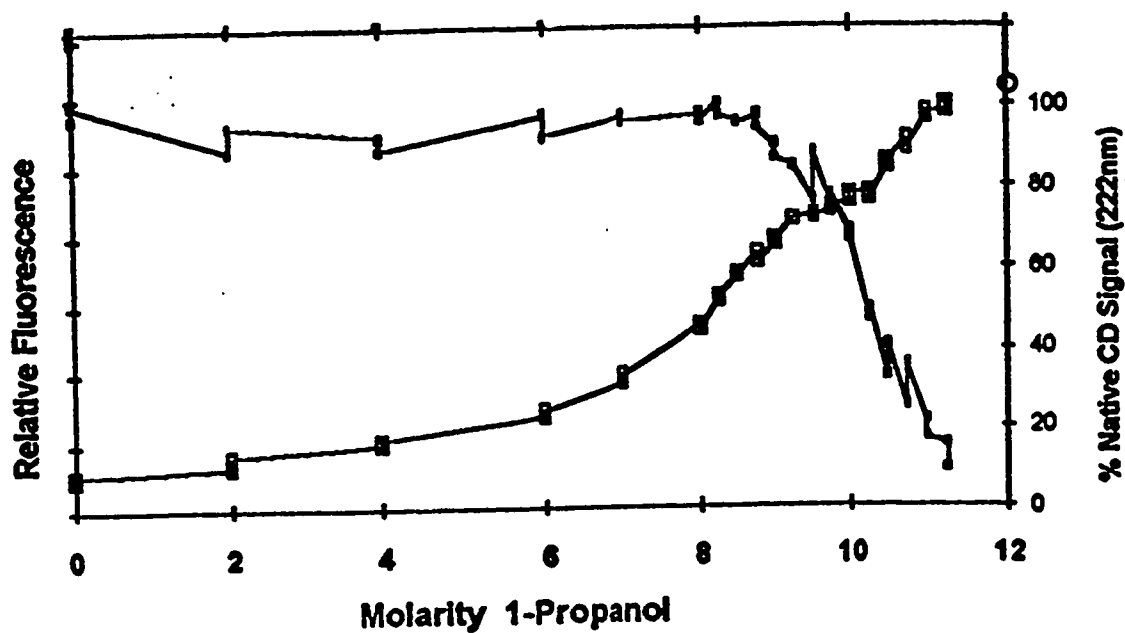


Figure 17: Fluorescence and CD of 1-propanol at $p_{a_{H^+}}$ 4.00. Denaturation of RNase A (18 μ M) by 1-propanol as monitored by intrinsic fluorescence (- \square - 280/305 nm) and circular dichroism (CD - \square - 222 nm) at $p_{a_{H^+}}$ 4.0, 0.05 M acetate buffer and 17 $^{\circ}$ C. The open circle on the right axis indicates the fluorescence obtained from RNase A denatured in 5.7 M guanidinium chloride at the same temperature and protonic activity.

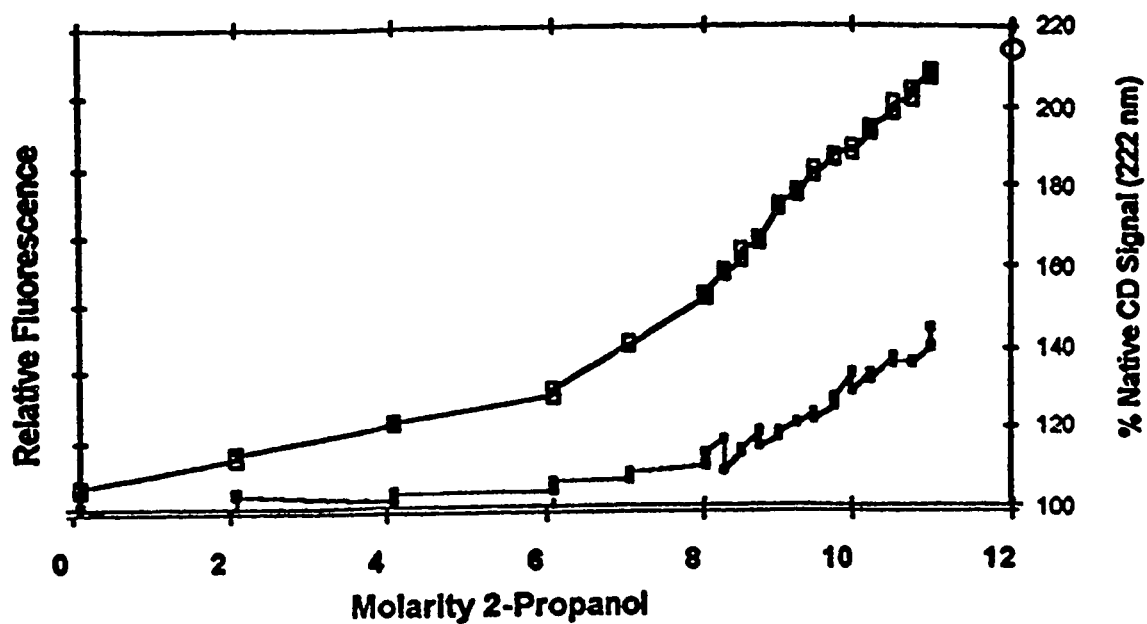


Figure 18: Fluorescence and CD of 2-propanol at p_{H^+} 3.00. Denaturation of RNase A (18 μM) by 2-propanol as monitored by intrinsic fluorescence (- \square - 280/305 nm) and circular dichroism (CD - \blacksquare - 222 nm) at p_{H^+} 3.0, 0.05 M formate buffer and 17 $^{\circ}\text{C}$. The open circle on the right axis indicates the fluorescence obtained from RNase A denatured in 5.7 M guanidinium chloride at the same temperature and protonic activity.

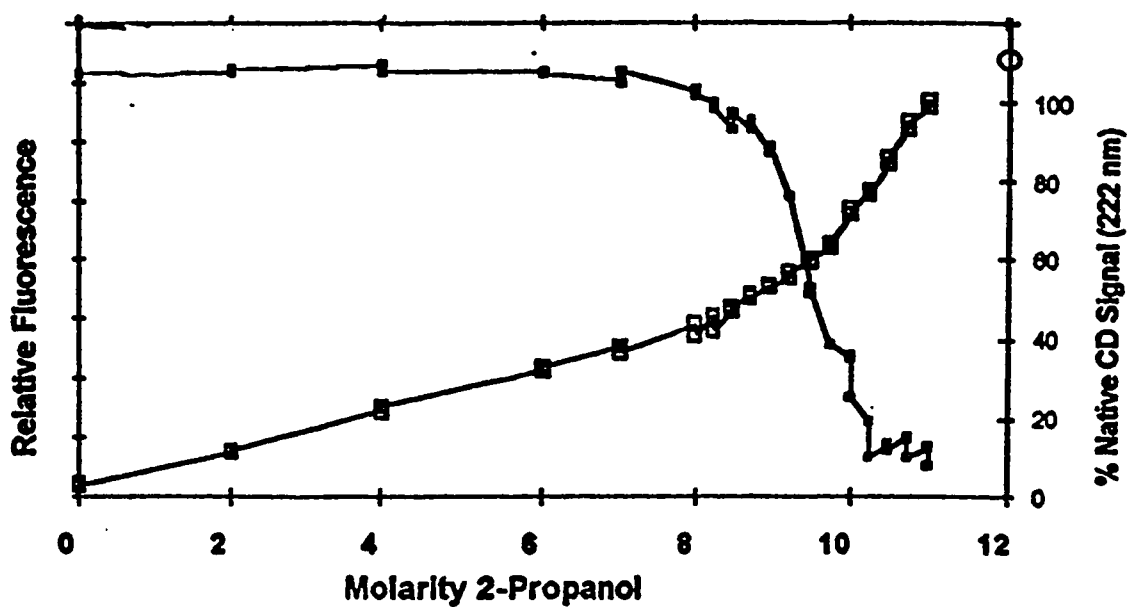


Figure 19: Fluorescence and CD of 2-propanol at $p_{a_{H^+}}$ 4.00. Denaturation of RNase A (18 μ M) by 2-propanol as monitored by intrinsic fluorescence (-■- 280/305 nm) and circular dichroism (CD -●- 222 nm) at $p_{a_{H^+}}$ 4.0, 0.05 M acetate buffer and 17 °C. The open circle on the right axis indicates the fluorescence obtained from RNase A denatured in 6 M guanidinium chloride at the same temperature and protonic activity.

the alcohols, which indicates a loss in the secondary structure. Comparison to the fluorescence data indicates that a loss in the tertiary structure is concomitant with a loss in the secondary structure. Evaluation of the data revealed a linear dependence of ΔG on the molarity of alcohol. This allowed for the evaluation of C_m values by the linear extrapolation methods described above. They were found to be 10 M and 9.5 M for 1-propanol and 2-propanol respectively.

The propanol-mediated denaturations at $p_{a_{H^+}}$ 3.00, as monitored by far UV-CD, are shown in Figures 16 and 18. The data for both alcohols show an increase in the ellipticity at 222 nm with increasing alcohol concentration. Comparison to the corresponding fluorescence data indicates that the loss of tertiary structure is accompanied by an increase in the secondary structure. The transition midpoints for the CD data were not calculated for $p_{a_{H^+}}$ 3.00, as an increase in the signal was observed at 222 nm, and thus no comparative standard is available.

3.3 Aggregation

At $p_{a_{H^+}}$ 4.00, significant aggregation was observed for all of the alcohols at higher concentrations and no aggregation was observed at $p_{a_{H^+}}$ 3.00 at any alcohol concentration used in this study. The aggregation at $p_{a_{H^+}}$ 4.00 was observed in the form of slight turbidity in protein solution. The onset of aggregation began at 22.5 M for methanol, and 11.25 M for both 1- and 2-propanol. Thus, all the fluorescence and far UV-CD measurements were limited to 22 M for methanol and 11 M for both 1- and 2-propanols solutions.

3.4 Singular Value Decomposition Analysis

In Figure 20, the percent secondary structure versus molarity of methanol for α -helix, antiparallel β -sheet, and parallel β -sheet is plotted. The data obtained at low concentrations of methanol (0-15 M) was obtained by using 360 μ M RNase A (Biringer, unpublished data). The data shows that the α -helix and antiparallel β -sheet content increases with an increase in the concentration of the alcohol, whereas parallel β -sheet remains unchanged even at high concentrations of alcohol. The data obtained for turn and other structures were too scattered to be of use.

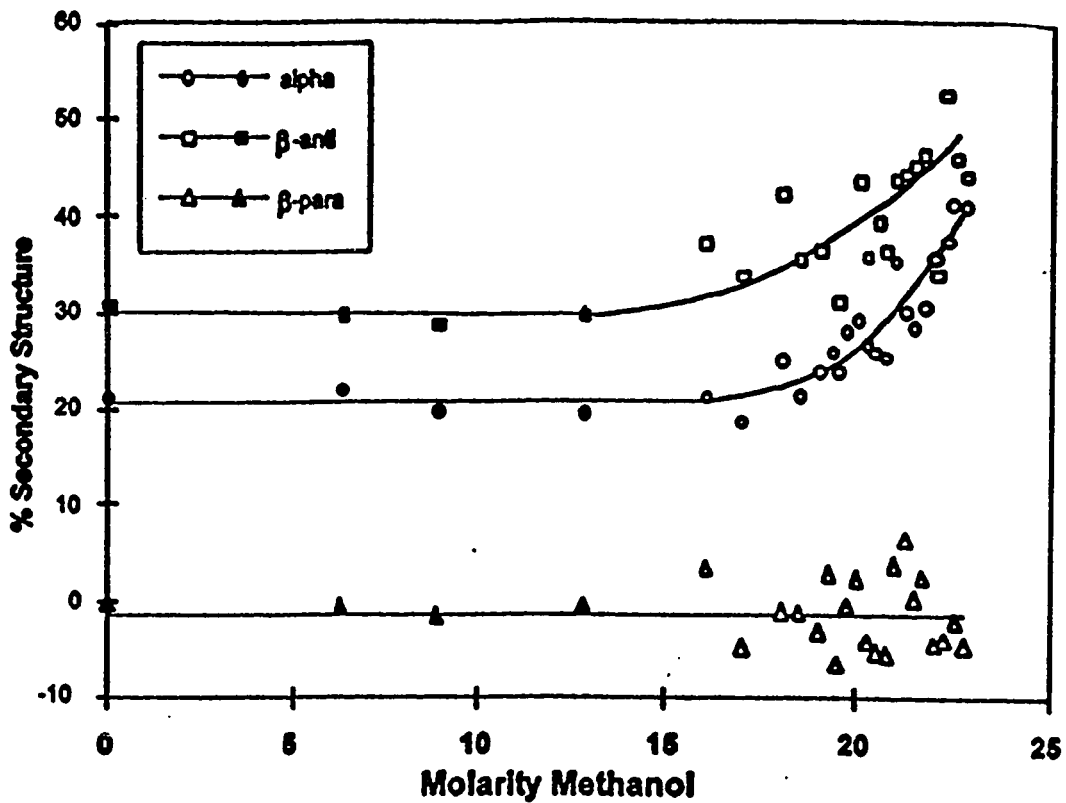


Figure 20: Singular value decomposition analysis data. Singular value decomposition analysis (SVD) of CD spectra for RNase A in methanol at 17 °C and p_{aH^+} 3.0. Results are given for α -helix, antiparallel β -sheet and parallel β -sheet. Open symbols give data for 18 μ M RNase A and closed symbols for 360 μ M RNase A. Curves drawn through data have no statistical meaning.

4.0 DISCUSSION

4.1 Fluorescence Studies

In this study of the chemical denaturation of RNase A by monohydric alcohols, fluorescence spectroscopy was used to monitor protein denaturation as a function of solvent composition. Figures 13, 14, and 16-19 show the unfolding transitions for RNase A for all the denaturants at p_{H^+} 3.00 and 4.00. Evaluation of the fluorescence-monitored denaturations under all conditions gave the expected increase in fluorescence emission associated with solvent exposure of the tyrosine residues.

The complete denaturation profiles could not be obtained for the reasons noted previously (section 3.2.1). In order to characterize the denatured state of a protein, the data was compared to the fluorescence obtained from RNase A denatured in 5.7 M guanidinium chloride and the appropriate p_{H^+} . The results show that at least 95% of the fluorescence transition was observed for each alcohol examined.

4.2 Transition Midpoints

The transition midpoints for the fluorescence data under all conditions were estimated from the raw data and are summarized in Table 1. The C_m values obtained for the propanols were between 9-10 M while that for methanol was 21 M. These concentrations of alcohol correspond to mole fractions of 0.52 and 0.68 respectively. This indicates that the transition midpoints decrease with an increase in the chain length and thus hydrophobicity of the alcohol.

Table 1: TRANSITION MIDPOINTS

	fluorescence		CD	
	p _H + 3.0	p _H + 4.0	p _H + 3.0	p _H + 4.0
Methanol	21	21	ND	ND
1-Propanol	10	9-10	ND	10
2-Propanol	9.5	10.5	ND	9.5

Transition midpoints for fluorescence data were estimated from the raw data. Transition midpoints for CD data were evaluated using linear extrapolation methods. Transition midpoints for CD data were not determined (ND) for those transitions where an increase in signal was observed.

The trend observed in transition midpoints is comparable to the results obtained by Schrier et al. (1965). In their study on effect of alcohol on thermal transition of ribonuclease, they observed a decrease in thermal stability as the chain length of the alcohol increased. According to Schrier et al. (1965) the lowering of the transition temperature of RNase A with alcohol chain length is largely entropy dependent. They concluded that the reduction in the transition temperature was the result of the binding between the nonpolar portion of the alcohol molecule and the exposed hydrophobic regions on the fully denatured protein. Their results were interpreted in terms of a stoichiometric binding of alcohol molecules to independent sites on the fully denatured protein. Thus, the alcohols denature the protein by weakening or disrupting the hydrophobic bonds between the side chains. In other words, the nonpolar side chains, which are exposed to solvent by unfolding, have a lower free energy in alcohol/water mixtures than in water alone.

Evaluation of the fluorescence-monitored transitions by the linear extrapolation method show a nonlinear dependence of ΔG with respect to alcohol concentration for all the alcohols examined. This is consistent with the formation of a population of partially-folded intermediate states within the transition region. Thus, all fluorescence-monitored transitions do not fit the two-state model as observed for RNase A in other denaturation studies. There are a number of protein-folding models which postulate the formation of compact, partially-folded structures in the folding pathway, and the fluorescent results presented here support these (Kuwajima, 1989; Kim and Baldwin, 1990). Our working

model is:



where I is the intermediate state. According to this scheme, the conversion from I to U occurs within the transition region of the denaturation curve. Attempts were made to curve fit the data to a three-state model, but were not successful. This suggests that either the equilibrium constants for the two processes are very close to one another, or the concentration of the intermediate is low. Thus, further characterization of these individual states could not be facilitated.

4.3 Circular Dichroism Studies

Figures 13, 14, and 16-19 show the far UV-CD data as monitored at 222 nm. Far UV-CD signals were examined in order to assess the secondary structure of the protein. It is clear from Figures 17 and 19 that at $p_{a_{H^+}} 4.00$, with an increase in the concentration of the 1- and 2-propanols, the observed ellipticity at 222 nm decreases to zero. Thus, the loss of the tertiary structure accompanies the loss of secondary structure in the propanol-mediated denaturations at $p_{a_{H^+}} 4.00$. Unlike the fluorescence data, the far UV-CD data obtained from the propanol-mediated denaturations at $p_{a_{H^+}} 4.00$, follows the two-state model, since the plots of free energy (ΔG) vs M propanols were linear in the transition region. The transition midpoints for the CD data corresponding to the propanols at $p_{a_{H^+}} 4.00$ shown in Table 1 were evaluated using the linear extrapolation method. Since the CD transition follows a two-state model and the fluorescence data a multistate model, the CD transition can only represent one of the two transitions observed by fluorescence. The

particular fluorescence transition that it is associated with cannot be determined at this time, as the C_m values for the individual transitions could not be obtained from the fluorescence data.

In contrast, the far UV-CD data obtained from the methanol-mediated denaturation at $p_{a_{H^+}}$ 4.00 shows very little change in the secondary structure (Figure 14). Thus, in the methanol-mediated denaturations at $p_{a_{H^+}}$ 4.00, the loss of tertiary structure is not accompanied by a decrease or increase in secondary structure. This result is consistent with the formation of an intermediate with the properties of a molten globule state where the protein lacks native tertiary structure, but retains native secondary structure.

All denaturation data at $p_{a_{H^+}}$ 3.00 show an increase in the amplitude of the CD signal at 222 nm, indicating that an increase in secondary structure is concomitant with the loss in the tertiary structure. Alcohols, being organic solvents, possess nonpolar groups and a lower dielectric constant than water. These two properties are considered important, as they promote α -helix formation. Alcohols are thought to increase intramolecular hydrogen bonding by decreasing the competition with water and enhance both the electrostatic and dipolar interactions within the protein by reducing the dielectric of the medium (Leroy and Jonas, 1994). Conio et al. (1970) observed that aliphatic alcohols enhances the stability of helices of poly-L-ornithine and poly-L-glutamic acid. Parodi et al. (1973) examined the thermal denaturation of lysozyme in aqueous aliphatic alcohol solutions. They found that low concentrations of alcohols do not stabilize α -helix, but higher concentrations do. These results are similar to those obtained in this study at $p_{a_{H^+}}$

3.00 (Figure 13, 16, 18).

4.4 Singular Value Decomposition Analysis

The increase in CD signal observed at p_{aH^+} 3.00 can be interpreted in a number of ways. One possibility is that random or other secondary structure may be converted to α -helices. Lapanje and Kranjc (1982) have observed the conversions of β -sheet to α -helices in the alkylurea mediated denaturation of β -lactoglobulin. The increase in the CD signal could also be due to an enhanced stabilization of the native α -helices. Also, the molar ellipticities for both the α - and β structures may just be larger in lower dielectric solvent. In order to address this, singular value decomposition analysis was performed to characterize the increase in the CD signal at 222 nm.

SVD analysis of the CD spectra for the methanol-mediated denaturation at p_{aH^+} 3.00 (Figure 20) shows an increase in the contribution from both α -helix and antiparallel β -sheet. The contribution from parallel β -sheet remains unchanged throughout since this structure is not found in the native RNase A. This result suggests that the formation of nonnative secondary structure is not responsible for the increase in the CD signal. The increase in the contribution from both α -helix and antiparallel β -sheet eliminates the possibility of sheet-helix conversion.

Thermal denaturation studies conducted by Lustig and Fink (1992) suggests that SVD analysis is valid for RNase A in 50% v/v methanol. This suggests that a solvent effect on the molar ellipticities is not responsible for the observed results.

By the process of elimination, the most likely explanation is that the α -helix found

in native RNase A is stabilized by high concentrations of alcohols. In aqueous solutions, the helices open and close constantly due to the dynamic movements in the protein structure. Alcohols, due to their ability to stabilize the formation of α -helices, shift the equilibrium to fully coiled state thereby reducing the extent of breathing movements.

4.5 Aggregation

The aggregation observed at $p_{a_{H^+}}$ 4.00 was rather surprising, as one would expect the denatured state, with its exposed hydrophobic groups, to be more soluble at higher alcohol concentration than lower concentration. Since the dielectric constant of the solution decreases with increasing alcohol concentration and electrostatic and dipolar forces increase with decreasing dielectric, the electrostatic and dipolar attraction or repulsion between protein molecules will increase with increasing alcohol concentration. It is possible that high concentrations of alcohols enhance the electrostatic or dipolar attraction between protein molecules to the point where these forces are stronger than the hydrophobic attractive forces between the protein and the alcohol molecules.

Since the protein molecules are more highly charged at $p_{a_{H^+}}$ 3.00 than at $p_{a_{H^+}}$ 4.00 and aggregation is not observed at pH^* 3.00, the stronger electrostatic repulsion apparently destabilizes the aggregate structure at $p_{a_{H^+}}$ 3.00. This suggests that the intermolecular attraction must be due to dipolar forces, in particular, hydrogen bonding. Yang et al. (1994) have examined the formation of dimeric and trimeric aggregates of Lysozyme-derived peptides. Their results are consistent with the formation of intermolecular β -sheet. In the β -sheet form, the solubility of the peptide is decreased

leading to an aggregation of the peptide. Yang et al. (1994) have shown that the β -sheet structure is associated with the formation of trimers and higher oligomeric forms of the peptide.

5. CONCLUSIONS

The most significant conclusion from this study is that transition midpoints decrease with an increase in the hydrophobicity of the alcohol denaturant. The C_m values obtained for the propanols were between 9-10 M and that for methanol was 21 M. The loss of tertiary structure accompanies a loss of secondary structure in the propanol-mediated denaturations at $p_{a_{H^+}}$ 4.00. This is typical for the denaturation of this and other proteins. In the methanol-mediated denaturation at $p_{a_{H^+}}$ 4.00, loss of tertiary structure is not accompanied by significant changes in secondary structure. This is consistent with the formation of a molten globule state.

Denaturation of RNase A with all alcohols at $p_{a_{H^+}}$ 3.00 show an interesting result in the form of an increase in secondary structure that follows the loss of tertiary structure. SVD analysis of the CD spectra for the methanol-mediated denaturation at $p_{a_{H^+}}$ 3.00 shows an increase in only those secondary structures found in the native RNase A. This leads to the conclusion that the enhanced secondary structure must be nativelylike.

Protein aggregation was observed at high alcohol concentration for all alcohols at $p_{a_{H^+}}$ 4.00, but not at $p_{a_{H^+}}$ 3.00. The $p_{a_{H^+}}$ dependence suggests that aggregation is the result of intermolecular hydrogen bonding between denatured protein molecules.

The nonlinear dependence of free energy ΔG , with respect to alcohol concentration for the fluorescence-monitored transitions indicate that the transitions do not fit the two-state model. The data support the population of at least one partially-folded intermediate state.

REFERENCES

- Baldwin, R. L. *Ann. Rev. Biochem.* **1975**, *44*, 453.
- Biringer, R. G. San Jose State University, unpublished results.
- Biringer, R. G.; Fink, A. L. *J. Mol. Biol.* **1982**, *22*, 381.
- Blum, A. D.; Smallcombe, S. H.; Baldwin, R. L. *J. Mol. Biol.* **1978**, *118*, 305.
- Chen, B. L.; Baase, W. A.; Nicholson, H.; Schellman, J. A. *Biochemistry* **1992**, *31*, 1464.
- Compton, L. A.; Johnson, C. W., Jr. *Anal. Biochem.* **1986**, *155*, 155.
- Creighton, T. E. In *Protein Folding*; L. M. Gierasch and J. King, Eds. AAAS, Washington, DC, 1990.
- Creighton, T. E. *J. Biochem.* **1990**, *270*, 1.
- Creighton, T. E.; Goldenberg, D. P. *J. Mol. Biol.* **1984**, *179*, 497.
- Dill, K. A. *Biochemistry* **1990**, *29*, 7133.
- Dill, K. A.; Fiebig, K. M.; Chan H. S.; *Proc. Natl. Acad. Sci. U.S.A.* **1993**, *90*, 1942.
- Dill, K. A.; Shortle, D. *Ann. Rev. Biochem.* **1991**, *60*, 795.
- Dym, O.; Mevarech, M.; Sussman, J. L. *Science* **1995**, *267*, 1344.
- Fink, A. L.; Calciano, L. J.; Goto, Y.; Kurotso, T.; Palleros, D. P. *Biochemistry* **1994**, *33*, 12504.
- Ghuman, R.; Henriquez, V.; Biringer, R. G.; San Jose State University, unpublished results.
- Goto, Y.; Calciano, L. J.; Fink, A. L. *Proc. Natl. Acad. Sci. U.S.A.* **1990**, *87*, 573.
- Jaenicke, R. *Biochemistry* **1991**, *30*, 3147.
- Karplus, M.; Weaver, D. L. *Protein Science* **1994**, *3*, 650.
- Kim, P. S.; Baldwin, R. L. *Ann. Rev. Biochem.* **1982**, *51*, 459.
- Kim, P. S.; Baldwin, R. L. *Ann. Rev. Biochem.* **1990**, *59*, 631.

- Kuwajima, K. *Proteins: Struct. Funct. Genet.* **1989**, *6*, 87.
- Labhardt, A. M. In *Protein Folding*; Ed.; Schenke, R., Proceedings of the 28th Conference of the German Biochemical Society: Elsevier, Amsterdam, **1980**; pp. 401-424.
- Lapanje, S.; Kranjc, Z. *Biochim. Biophys. Acta.* **1982**, *705*, 111.
- Levitt, M. J. *Mol. Biol.* **1976**, *104*, 59.
- Lustig, B.; Fink, A. L. *Biochim Biophys. Acta.* **1992**, *1119*, 205.
- Matthews, C. R. *Ann. Rev. Biochem.* **1993**, *62*, 653.
- Pace, C. N.; Laurents, D.V.; Thomson, J. A. *Biochemistry* **1990**, *29*, 2564.
- Pace, C. N.; Marshall, H. F., Jr. *Arch. Biochem. Biophys.* **1980**, *199*, 270
- Privalov, P. L. *CRC Crit. Rev. Biochem. Mol. Biol.* **1990**, *25*, 281.
- Privalov, P. L.; Gill, S. J. *Adv. Protein. Chem.* **1988**, *39*, 193.
- Privalov, P. L.; Gill, S. J. *Pure Appl. Chem.* **1989**, *61*, 1097.
- Privalov, P. L. In *Protein Folding*; Creighton, T. E., Ed.; W. H. Freeman and Co: NewYork, 1992; Chapter 3, pp. 83-126.
- Ptitsyn, O. B. In *Protein Folding*; Creighton, T. E., Ed.; W. H. Freeman and Co: NewYork, 1992; Chapter 6, pp. 269-280.
- Sage, H. J.; Singer, S. J. *Biochemistry*, **1962**, *1*, 305.
- Santoro, M. M.; Bolen, D. W. *Biochemistry* **1988**, *27*, 8063.
- Schellman, J. A. *Biopolymers* **1987**, *26*, 549.
- Schmid, F. X.; Baldwin R. L. *J. Mol. Biol.* **1979**, *133*, 285.
- Schmid, F. X. *Ann. Rev. Biophys. Biomol. Struct.* **1993**, *22*, 123.
- Schrier, E. E .; Ingwall, R. T.; Scheraga, H. A. *J. Chem. Phy.* **1965**, *69*, 298.
- Seckler, R.; Jaenicke, R. *FASEB Jour.* **1992**, *6*, 2545.
- Shortle, D.; Meeker, A. K. *Biochemistry* **1989**, *28*, 936.
- Singer, S. J. *Adv. Prot. Chem.* **1962**, *17*, 1.

Stigter, D.; Dill, K. A. *Biochemistry* **1990**, *29*, 1262.

Stryer, L. *Science* **1968**, *162*, 526.

Tanford, C. *Adv. Prot. Chem.* **1968**, *23*, 121.

Udgaonkar, J. B.; Baldwin, R. L. *Nature* **1988**, *335*, 694.

von Hippel, P. H.; Schleich, T. *Acc. Chem. Res.* **1969**, *2*, 257.

Wetlaufer, D. B. (1973) *Proc. Natl. Acad. Sci. U.S.A.* **1973**, *70*, 697.

Wu, H. (1929) *Am. J. Physiol.* **1929**, *90*, 562.

Yang, J. J.; Pitkeathly, M.; Radford, S. E. *Biochemistry* **1994**, *33*, 7345.

**PERMISSION TO REPRODUCE
IN DISSERTATION**

July 1, 1995

Sujatha Subbiah
Dept. of Chemistry
San Jose State University
One Washington Square
San Jose, Calif. 95192-0101



**CAMBRIDGE
UNIVERSITY PRESS**

North American Branch
40 West 20th Street
New York, NY 10011-4211
USA

Telephone 212 924 3900
Fax 212 691 3239

Reference

ISBN or Journal: *Protein Science*, Vol. 3 (1994)
Author: Karplus, Martin and Weaver, David L.
Title: "Protein Folding Dynamics: The Diffusion-collision Model
and Experimental Data"
Item/pp.: Fig. 1, p. 352, only

Use

University/College: San Jose State University

Rights/Acknowledgement

Permission is granted for non-profit educational use in one dissertation only, subject to full acknowledgement of our material and clear indication of the copyright notice as it appears in our publication, followed by the phrase "Reprinted with the permission of Cambridge University Press." This permission is restricted to print (paper) reproduction and excludes electronic reproduction in any other medium, or reprinting in any formal publication (e.g., book/periodical/newspaper), in any medium, for which permission must be requested separately. The rights granted herein may not be re-assigned in any manner to any other person, company or organization for any other purpose.

Restrictions

This permission does not allow reprinting any material copyrighted by or credited in our publication to another source; to use such material, permission must be obtained directly from the owner of that material.

Authorization:

A handwritten signature in black ink, appearing to read "M.P. Anderson", written over a horizontal line.

M.P. Anderson
Manager, Rights and Permissions

From
Sujatha Subbiah,
Department of Chemistry,
San Jose State University,
San Jose, CA-95192-0101.

To
National Academy of Sciences,
Proceedings office,
2101, Constitution Av, N. W.,
Washington D. C. -20418.

Sir / Madam,

I am a graduate student at San Jose State University, San Jose- CA, finishing up with M. S. in Chemistry. I want to include a figure (Figure 1 p:1942) from the journal **Proc. Natl. Acad. Sci. USA, vol.90, pp.1942-1946, March 1993** entitled "Cooperativity in Protein-Folding kinetics" by Ken A. Dill, Klaus M. Fiebig, and Hue Sun Chan in my M. S. thesis. I would like to let you know that three copies of my thesis would be published. I would like to receive a written permission from you in this regard.

With regards,

Yours truly,

Sujatha Subbiah

*Permission granted
Franco R. Juretzik
June 21, 1995
Please cite as "copyright National Academy of
Sciences USA"*

41 MADISON AVENUE, NEW YORK, NEW YORK 10010
TELEPHONE: (212) 576-9400
FAX: (212) 689-2383

AGREEMENT FOR PERMISSION TO REPRINT

To: Sujatha Subbiah

Date: 18 July 1995

From: Katherine Loughran

**THIS FORM MUST BE SIGNED AND ALL COPIES RETURNED TO THE PERMISSIONS DEPARTMENT.
THIS PERMISSION IS NOT VALID UNLESS IT IS SIGNED BY BOTH PARTIES.**

The undersigned requests a non-exclusive license to reprint the following selection(s):

TITLE: PROTEIN FOLDING

Figure 6-6

AUTHOR: Creighton

To be used in: the thesis of _____ by: Subbiah

Address: San Jose State University, Dept of Chemistry, San Jose, CA 95192

To be published by: _____ Probable retail price: _____
Hardcover/Paperback Text/Trade/Other Approx. date of publication: _____

The undersigned agrees as follows:

- 1) Full credit in every copy printed, on the copyright page or in the caption, or as a footnote on the page on which the quotation/illustration appears, or if in a magazine or journal, on the first page of each quotation/illustration covered by the permission, or scrolled at the end of the program, videodisc or CD-ROM exactly as follows:
From: **PROTEIN FOLDING** by Creighton. Copyright (c) 1992 by W.H. Freeman and Company. Used with permission.
- 2) To pay on publication of the work, or within 24 months of the date of granting the permission, whichever is earlier, a fee of:
No fee ✓
- 3) Payment must be accompanied by one copy of the licensing agreement and one copy of the published work to ATTN: PERMISSIONS DEPARTMENT, W.H. Freeman and Company.
- 4) The permission granted applies only to the edition of the work specified in this agreement and is not transferable.
- 5) This license is valid for a period of seven years from the date of publication of the work named herein.
- 6) This permission applies, unless otherwise stated, solely to the publication of the above-cited work in the English language.
- 7) This permission does not extend to any copyrighted material from other sources which may be incorporated in the works in question, nor to any illustrations or charts, unless otherwise specified.
- 8) This selection may be reproduced in Braille, large type, and sound recordings provided no charge is made to the visually handicapped.
- 9) **This agreement must be returned within 120 days from the date above or the permission shall automatically terminate.**

Date: July 25th, 1995 Signature of Applicant: Sujatha

Address: 1180, Lochinvar Ave #108, Sunnyvale, CA-94087

Date: August 2, 1995

Permission on the foregoing terms
W.H. FREEMAN AND COMPANY
By Nancy Walker
Permissions Department